Structural geology of the Gullfaks Field, northern North Sea

HAAKON FOSSEN[1] & JONNY HESTHAMMER[2]

[1]*Department of Geology, University of Bergen, Allégt. 41, N-5007 Bergen, Norway*
[2]*Statoil, N-5020 Bergen, Norway*

Abstract: The large amount of structural data available from the Gullfaks Field have been used to unravel the structural characteristics of the area. Two structurally distinct sub-areas have been revealed (a major domino system and an eastern horst complex) that show significant differences with respect to fault geometry, rotation and internal block deformation. The main faults have very low dips in the domino system (25–30°) as compared to the horst complex (65°), whereas most minor faults are steep in all parts of the field. Forward modelling indicates that the horst complex balances with rigid block operations. However, the domino area underwent significant internal deformation, reflected by the low acute angle between bedding and faults, and by non-planar bedding geometries. The internal deformation is modelled as a shear synthetic to, but steeper than, the main domino faults. This deformation explains a large-scale (kilometre sized) drag zone that has a triangular geometry in cross-section. Much of this shear deformation occurred by strain-dependent grain reorganization in the poorly consolidated Jurassic sediments, which led to a decrease in porosity. A strain map is presented for the domino area, indicating where the porosity is likely to have been decreased due to internal shear. Hangingwalls are generally more deformed (sheared) than footwalls. This is seen on both the kilometre scale (large-scale drag) and the metre scale (local drag).

There has been a rapidly growing interest in understanding extensional crustal deformation at various scales during the last few decades. Common approaches include physical modelling (Horsfield 1977; McClay & Ellis 1987; Vendeville *et al.* 1987; Withjack *et al.* 1995), theoretical/numerical modelling (Jarvis & McKenzie 1980; Houseman & England 1986; Kusznir & Ziegler 1992; Childs *et al.* 1990), seismic studies (Blundell *et al.* 1985; Beach 1986; Klemperer 1988) and field studies (Jackson *et al.* 1988; Davison *et al.* 1994). While theoretical and physical modelling are indeed important tools, they must be guided by and tested against data and observations of naturally deformed rocks. Detailed observations and careful collection of field data are therefore crucial.

Although some well-exposed portions of rift systems do exist (e.g. the gulfs of Corinth and Suez), most rift systems are buried by syn-rift or post-rift sedimentary sequences and/or water. Exposed examples may have been brought to the surface by contractional crustal movements, causing reactivation and reworking of the original extensional structures. However, an overwhelming amount of geological and geophysical data have accumulated in parts of rift systems where moderate to large oil-fields are located. We believe that systematic and integrated structural analysis of the various types of geo-data available from oil-fields in the North Sea and elsewhere is a key not only to improving well planning and reservoir management in the region, but also to increasing our general understanding of extensional deformation.

The present work is a contribution from the Gullfaks Oil-field in the North Sea, where more than 170 wells have been drilled and extensive well data of various types are collected. In addition, three-dimensional (3D) seismic data have recently been reprocessed and reinterpreted together with other field data in an integrated process. It represents an attempt to use and combine the many different types of data that are available from a producing oil-field to obtain the best understanding possible of the structural geology of the area.

Regional setting

The Gullfaks Field is located on the western flank of the Viking Graben (Fig. 1), where it occupies the eastern half of a 10–25 km wide, NNE–SSW-trending fault block named the Gullfaks fault block in this article. The Gullfaks fault block is one of a series of large (first-order) fault blocks that are easily identified on regional seismic lines across the North Sea. The general trend of these larger faults in the northern North Sea is N–S to NNE–SSW, reflecting the overall E–W extension across the rift.

The extensional history of the North Sea dates back to the Devonian extensional phase shortly after the Caledonian collision (e.g. McClay *et al.* 1986). Onshore kinematic studies support the

FOSSEN, H. & HESTHAMMER, J. 1998. Structural geology of the Gullfaks Field, northern North Sea. *In*: COWARD, M. P., DALTABAN, T. S. & JOHNSON, H. (eds) *Structural Geology in Reservoir Characterization*. Geological Society, London, Special Publications, **127**, 231–261.

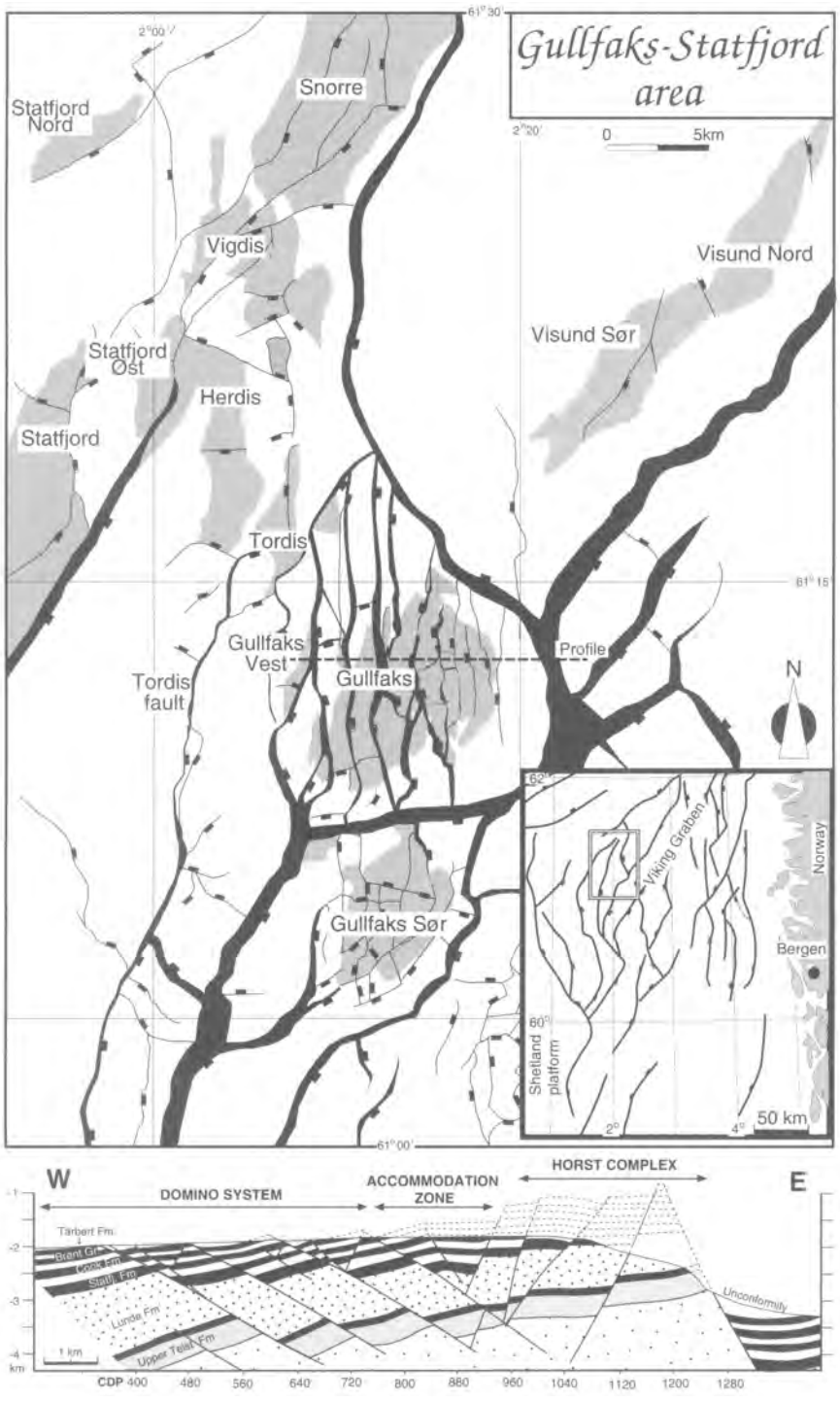

Fig. 1. Regional map of the northern North Sea (inset map) and of the Gullfaks–Statfjord area, and a profile across the Gullfaks Field.

idea of plate-scale divergent movements in the Devonian (Fossen 1992). The main subsequent rifting phases are commonly referred to as the Permo-Triassic and late Jurassic phases (e.g. Badley *et al.* 1988; Gabrielsen *et al.* 1990). Whereas the extension involved in the Permo-Triassic event is significant (Roberts *et al.* 1995), the late Jurassic deformation of the Jurassic sequence is more obvious on commercial seismic lines, and best known from well data. The present study is concerned with deformation of Late Triassic–Jurassic layers in the Gullfaks area, and thus with the late Jurassic extension phase.

The Gullfaks Field

The Gullfaks Field (Petterson *et al.* 1990) is situated east of the Statfjord Field and south of the Snorre Field (Fig. 1), and has been under production since 1986. Covering an area of *c.* 75 km^2, the field is developed by three concrete platforms under a fully Norwegian license group consisting of Statoil (operator), Norsk Hydro a.s. and Saga Petroleum a.s. Total recoverable reserves amount to about 310×10^6 Sm^3 of oil and some 30×10^9 Sm^3 of gas, located in the Jurassic Brent Group, Cook Formation and Statfjord Formation.

Stratigraphy

The deepest well in the Gullfaks area (34/10-13) was drilled to about 3350 m depth, and penetrated 1340 m of Triassic sands and shales of the Lunde and Lomvi Formations (Hegre Group). The base of the Triassic has never been reached in this part of the northern North Sea, and little is therefore known about early and pre-Triassic strata. From gravity surveys, palinspastic reconstructions and regional, deep-seismic lines, it is, however, inferred that only thin sequences of sediments are present between the Triassic clastics and Devonian or metamorphic/crystalline basement in this area.

The Triassic Hegre Group consists of interbedded intervals of sandstones, claystones and shales, all deposited in a continental environment. The upper part of the Hegre Group (the Lunde Formation) consists of medium-grained, fluvial sandstones and contains reserves in the eastern Gullfaks area. Overlying the Hegre Group is the Rhaetian–Sinemurian Statfjord Formation which consists of 180–200 m of sandstones deposited in an alluvial environment that changed its character from a well-drained semi-arid setting to a more humid alluvial plain.

The 370–420 m thick Dunlin Group is subdivided into the Amundsen, Burton, Cook and Drake Formations. The Amundsen and Burton Formations consist 170–180 m of marine claystones and siltstones overlain by the regressive, marine, silty claystones of the lower part of the 110–160 m thick Cook Formation, and in turn by muddy sandstones, sands and shales of the upper part of the Cook Formation. The 75–120 m thick Drake Formation comprises marine shales with varying amounts of silt.

The Brent Group of mainly Bajocian–Early Bathonian age forms the upper and main part of the reservoirs. It is sub-divided into the Broom (8–12 m), Rannoch (50–90 m), Etive (15–40 m), Ness (85–110 m) and Tarbert (75–105 m) Formations, all deposited in a deltaic environment. A broad lithological sub-division can be made between the shaly Ness Formation and the sandy intervals below and above.

A major time gap (up to 100 Ma) is represented by the base Cretaceous (late Cimmerian) unconformity on the Gullfaks Field, separating Upper Cretaceous sediments from Jurassic or Triassic sediments, and post-dating the major part of the faulting history of the area. Up to 100 m of Upper Jurassic shales (Heather Formation) are locally preserved in the hangingwalls to the main faults in the Gullfaks Field, particularly in the western part.

Structural outline

The Gullfaks Field is characterized by two structurally contrasting compartments (Fig. 1, profile): a western domino system with typical domino-style fault block geometry, and a deeply eroded eastern horst complex of elevated sub-horizontal layers and steep faults. These two regions are significantly different as far as structural development is concerned, and will be treated separately below. Between the western and eastern regions is a transitional accommodation zone (graben system) which is identified as a modified fold structure.

The distribution of these structurally different areas is shown in Fig. 2, which displays an east-stepping occurrence of the accommodation zone as one goes from the north to the south. The stepping occurs across E–W transfer faults with high displacement gradients (rapidly decreasing displacement to the west). These E–W faults thus separate domains of contrasting dips.

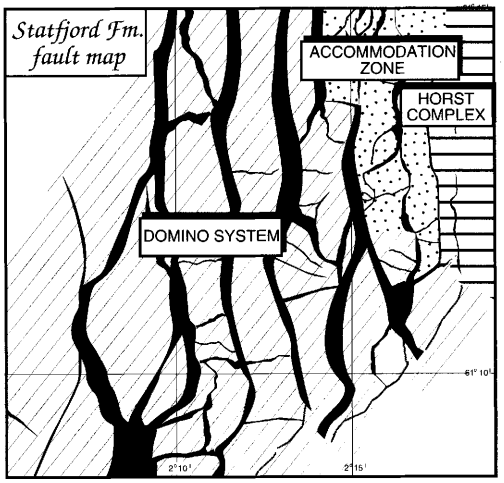

Fig. 2. The areal distribution of the domino system, the horst complex and the accommodation zone on the top Statfjord fault map.

Data and method

The structural analysis and discussion presented in this work are based on the multitude of exploration and production data from the Gullfaks Field. Ten thousand kilometres of reprocessed 3D seismic data (ST8511) were interpreted (1992–93). Reflections closely corresponding to base Cretaceous, top Rannoch Formation, top Amundsen Formation, top Statfjord Formation and an intra-Teist Formation were interpreted in the entire area. Other formation boundaries were partly interpreted and partly constructed from these formation boundaries by use of time-converted isochore maps. Seismic attribute maps, dipmeter data and other information from the approximately 170 wells through the Gullfaks reservoirs were used extensively during interpretation. Both the time-interpreted horizons and faults were depth-converted for structural analysis, using a linear velocity function combined with available well velocity (vertical seismic profile (VSP) and synthetic seismogram) information. The geometrical characteristics of the mapped formations (horizons) and faults are presented as maps, stereoplots and graphs that form a foundation for further analysis and discussion of the structural geology of the Gullfaks Field.

Two maps (top Rannoch and top Statfjord Formations, Figs 3 and 4) were selected for structural analysis, because they coincide or closely coincide with the best reflectors on the seismic lines, and they represent a significant (450 m) difference in depth. The orientation of the bedding was extracted by sub-dividing depth maps into squares of 312.5 m×312.5 m in which the average strike and dip of the bedding was estimated. Similarly, fault maps were sub-divided along strike into segments of 250 m length, and the average strike and dip were measured/calculated at or close to reservoir level (mostly at the Amundsen–Statfjord level). This length was found to be small enough to pick up all significant undulations in the fault plane geometry, and sufficiently large to even out some of the 'noise' that occurs from inaccurate interpretation (the faults were systematically interpreted every 100 m at the work station).

The domino area

The western domino region constitutes the main part of the Gullfaks Field. The deformation in this part of the field has resulted in a series of generally N–S-trending fault blocks. The faults defining these blocks are named F1, F2 etc. (see Fig. 5). They have displacements in the range 50–500 m, and will be termed main faults in this work. As will be discussed in more detail below, the block-bounding faults in this area have unusually low dips (25–30° to the east) whereas the sedimentary strata dip gently (typically about 15°) to the west. The domino fault blocks are compartmentalized by a series of smaller faults with throws generally below 50 m. These faults, which are referred to as minor faults, have more variable trends, including a marked E–W trend.

Geometry of main faults

Orientation data extracted from depth-converted fault contour maps of main faults were plotted in stereonets as poles to planes. The results (Fig. 6a–e) demonstrate well the non-planar geometry of the main faults, and the poles to the faults are remarkably well-distributed along great circles. The latter phenomenon, which was also noted by Koestler *et al.* (1992) for two faults in the western part of the domino area, reflects the cylindrical geometry of the non-planar faults at reservoir level. The poles to the best-fit great circles (β-axes of Ramsay (1967)) define the axis of curvature of the fault surfaces. Obviously, the easiest slip direction for the fault blocks is parallel to the β-axes. Movements oblique to this direction would imply serious compatibility problems which could be resolved only to a certain extent by internal deformation

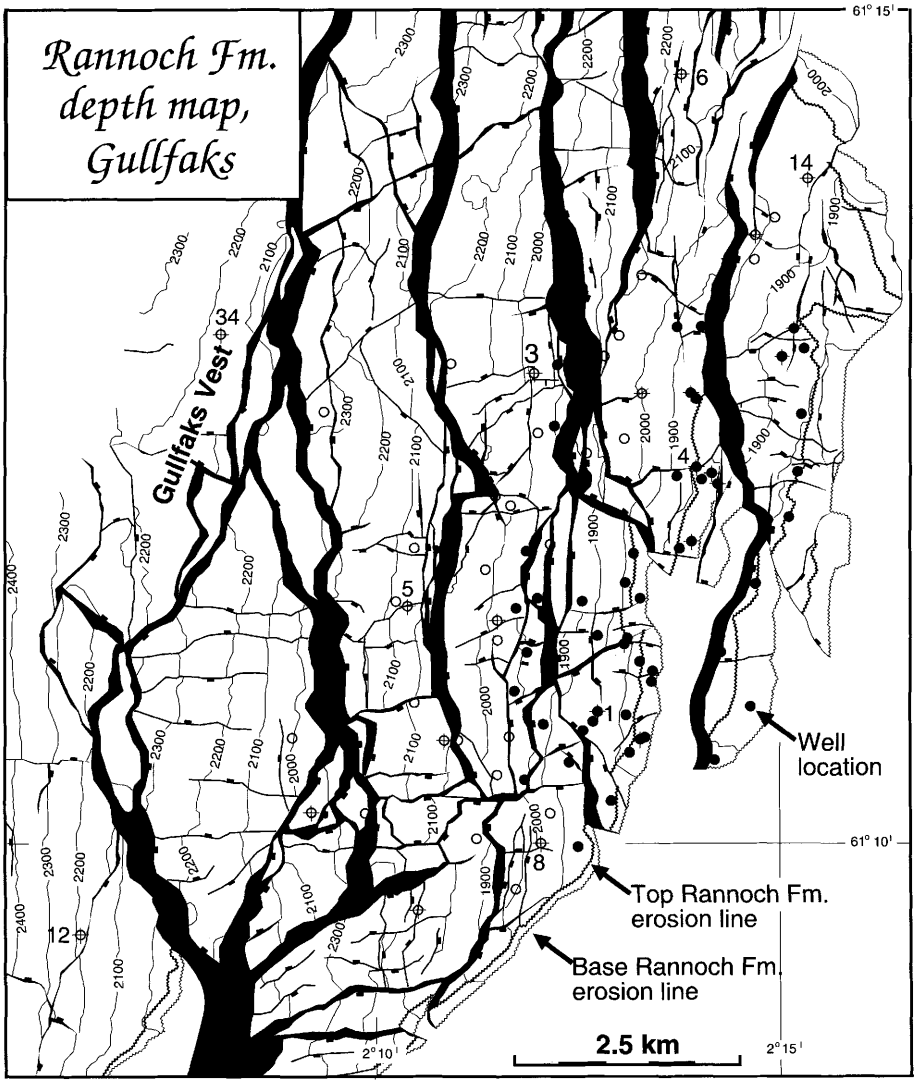

Fig. 3. Depth map of the Rannoch Formation in the Gullfaks Field.

near the fault. The poles to the best-fit great circles must therefore be close to the mean slip direction to the main faults. Figure 6 constrains the mean slip direction to an easterly trend (090 ± 10) with a plunge of about 25–30°. It can also be seen from Fig. 6a–e that the lowest dips (dips of N–S-striking fault segments) vary from 30° in the west to 25° in the east.

Geometry of minor faults

Minor faults show a much wider range in orientation than the main faults (Fig. 6f), and include: (1) N–S-striking minor faults sub-parallel (synthetic) to the main faults; (2) E–W-striking minor faults; (3) diagonal; and (4) steep N–S-striking minor faults antithetic to the main faults.

The first category have dips that are slightly steeper than the main faults if they occur in the hangingwall (hangingwall collapse, Fig. 7), and somewhat lower dips if they are related to footwall collapse. Hangingwall and footwall collapse have been mapped in several places, but may be difficult to identify from seismic data alone. Exploration of the Gullfaks Vest structure (Figs 3 and 4) is an example of the latter, where, after three pilots and two long horizontal wells,

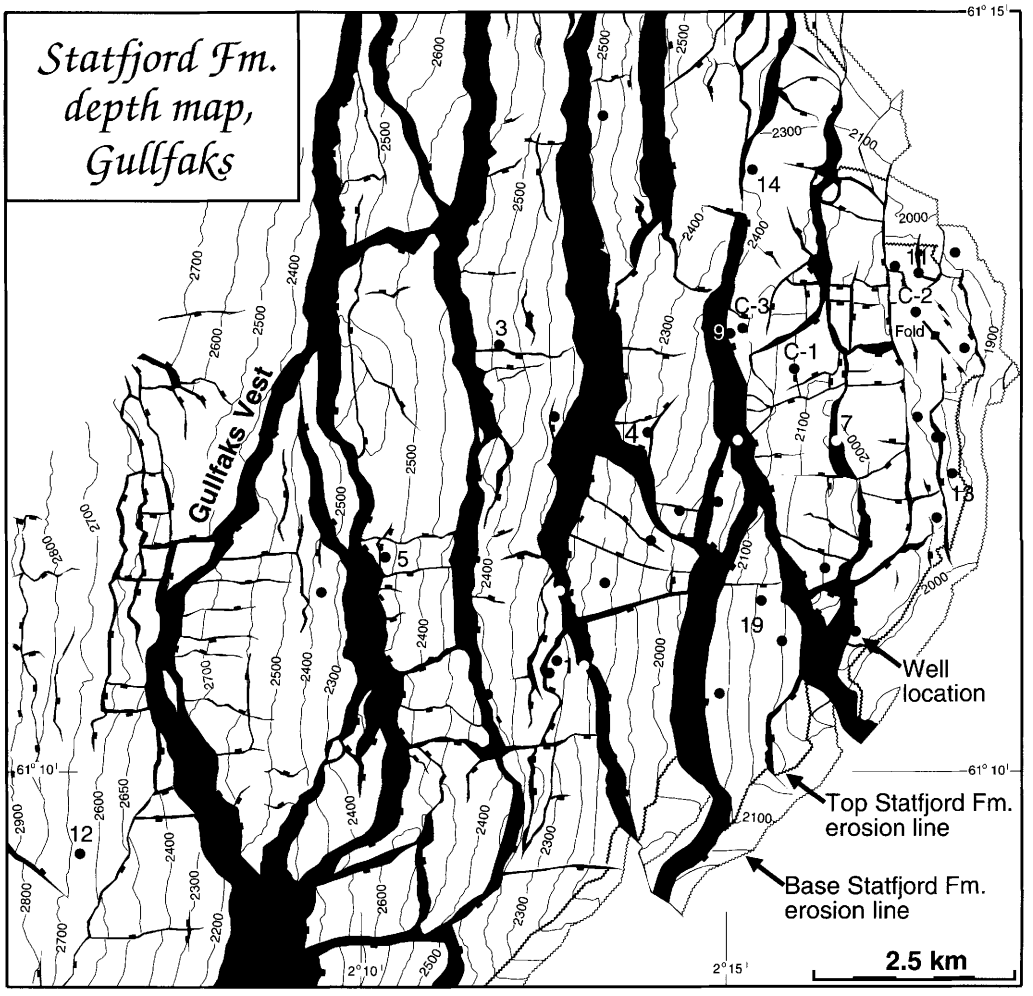

Fig. 4. Depth map of the Statfjord Formation in the Gullfaks Field.

the map pattern changed from a simple footwall geometry to a much more complex collapsed footwall rim. In this particular example, the collapse structures were largely restricted to the Brent Group (compare fault patterns of Figs 3 and 4), and were therefore not reflected in the well-defined but deeper Amundsen and Statfjord reflectors.

E–W-striking minor faults are typically steep (45–90°) and restricted to single domino blocks. They must therefore be related to internal block deformation, and are best interpreted as accommodation structures formed during a history of differential slip along the main faults. They are also characterized by small throws (many <20 m and almost all <50 m). From the stereographic projections (Fig. 6f) it appears that the N-dipping faults of this type are very steep, whereas a series of S-dipping E–W faults have somewhat lower (although still quite steep) dips.

Diagonal minor faults, i.e. NW–SE- or NE–SW-striking faults, are mapped in most of the Gullfaks area. These faults have variable throws and, like the other minor faults, most are restricted to single fault blocks. They have intermediate dips, and categories (1), (2) and (3) together define a great circle similar to the main faults (Fig. 6f).

Most antithetic faults are steep to sub-vertical and somewhat variable, but mostly N–S-striking. These faults have small (<20 m) throws, and are less common than the other

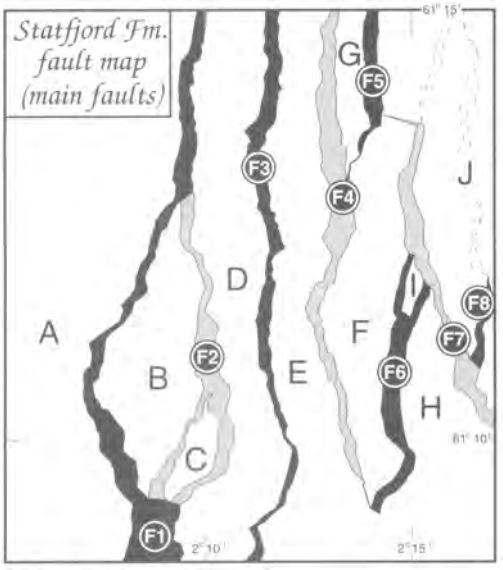

Fig. 5. Labelling of main faults and fault blocks on the Gullfaks Field.

types of minor faults. This expression of internal block deformation is interpreted as adjustment structures related to, for example, irregular block-boundary conditions.

Dipmeter data have proved useful for identification of sub-seismic minor faults. In order to identify small-scale faults by use of dipmeter data, a change in dip and/or dip direction of strata must exist. Such changes can occur as discrete discontinuities, or the changes may be gradual if drag exists (i.e. a deflection of layering adjacent to the fault surface).

Since the degree of bedding deflection around faults is related to fault dip, it is often possible to roughly estimate a minimum dip and dip direction of minor faults. Analysis of dipmeter data from the Gullfaks Field based on statistical curvature analysis techniques (Bengtson 1981) shows two major concentrations of dip directions of faults with drag: one to the east or southeast, and one to the west, i.e. synthetic and antithetic to the main domino faults (Fig. 8). The synthetic set appears to be more common. This corresponds to the higher number of synthetic than antithetic minor faults mapped on the seismic data (Figs 3, 4 and 6f). The E–W-striking minor faults identified from seismic interpretation are, however, not readily observed on dipmeter data, suggesting that they did not develop associated drag.

Fault zone characteristics

Analysis of core material has demonstrated the presence of a relatively narrow 'damage zone' along both major and minor faults, i.e. a zone with an anomalously high density of minor fractures. The width of such zones is typically less than 10 m for the minor faults, and apparently not much wider for the main faults.

On a somewhat larger scale, there is seismic and well evidence for minor faults that splay out from the main fault into the side walls to form hangingwall or footwall collapse structures (Fig. 7). In effect, these structures display an upward dissipation of deformation from the Statfjord Formation towards the base Cretaceous unconformity, i.e. the loose sands of the Brent Group responded differently to deformation than the deeper and more compacted strata. The deformation dissipation may therefore be the result of more active strain-hardening processes up-section during deformation.

Drag, i.e. deflection of bedding adjacent to the fault surface, is an expression of continuous or 'ductile' deformation near the fault, where the non-planar bedding in principle can be traced continuously through the drag zone. In the sense used here, the deformation associated with drag is microscopic, i.e. associated discrete (discontinuous) deformation is not visible in cores. This deformation is identifiable from dipmeter data, and analyses indicate that drag zones up to several tens of metres wide are developed for more than half of the faults that intersect wells with dipmeter data.

The common method of identifying faults from well-log correlation is by recognizing intervals of missing section. Since more than half of all faults on the Gullfaks Field have associated drag, it is clear that the 'total offset' (i.e. offset of a stratigraphic marker across the area affected by drag) will commonly be larger than the amount of missing section. In order to quantify the difference between 'total offset' and missing section, a profile was constructed through a drag zone identified from dipmeter data in the Amundsen Formation in well 34/10-C-3 (Fig. 9a). Dipmeter data suggest that the fault dips 45° or more to the west. Nine metres of missing section was identified from other well logs. Dip isogons were constructed parallel to the fault, thus assuming that the drag zone developed along a fault-parallel shear zone. The resulting profile shows that even though the missing section in the well is only 9 m, 'total offset' amounts to about 100 m in this extreme case. It is thus obvious that construction of geological profiles based on stratigraphic correlations

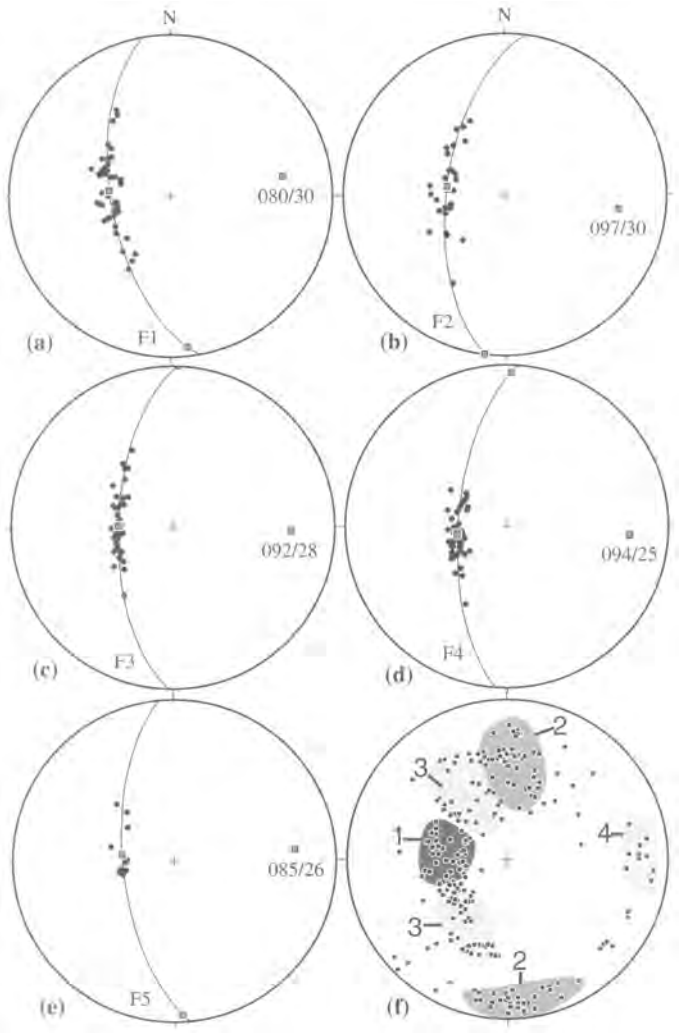

Fig. 6. Equal-area stereographic projections of poles to five main faults (F1–F5, see Fig. 5) (**a**)–(**e**) and minor faults in the domino area (**f**). The best-fit circle and its pole (calculated by Bingham analysis) are shown. The poles are expected to indicate the general slip direction associated with the main faults. The minor faults (f) are distinguished into four different groups: (1) minor faults synthetic to the main faults; (2) steep E–W-trending faults; (3) NE–SW and NW–SE-striking faults; and (4) sub-vertical N–S-trending faults.

alone can lead to serious under-estimates of displacement along faults. In addition, since drag may affect the geometry of the reservoirs, an improved understanding of drag may lead to more correct volume estimates and identification of unknown hydrocarbon prospects.

Drag zones around faults have been determined from dipmeter analysis to be less than 100 m wide. The drag zone is consistently wider in the hangingwall than in the footwall to faults (Fig. 9b), indicating stronger deformation of the hangingwall side of the fault.

Geometry of bedding

The bedding orientation data in the domino area were treated individually for each domino fault block (Fig. 5). Because of the low dips of the bedding, these data are best displayed as dip azimuth/dip plots rather than plots of poles to bedding.

Figures 10 and 11 show that the orientation of the bedding is fairly constant within each fault block as well as between the blocks. The average dips of the top of the Rannoch and Statfjord Formations are 13° and 16.6°, respectively

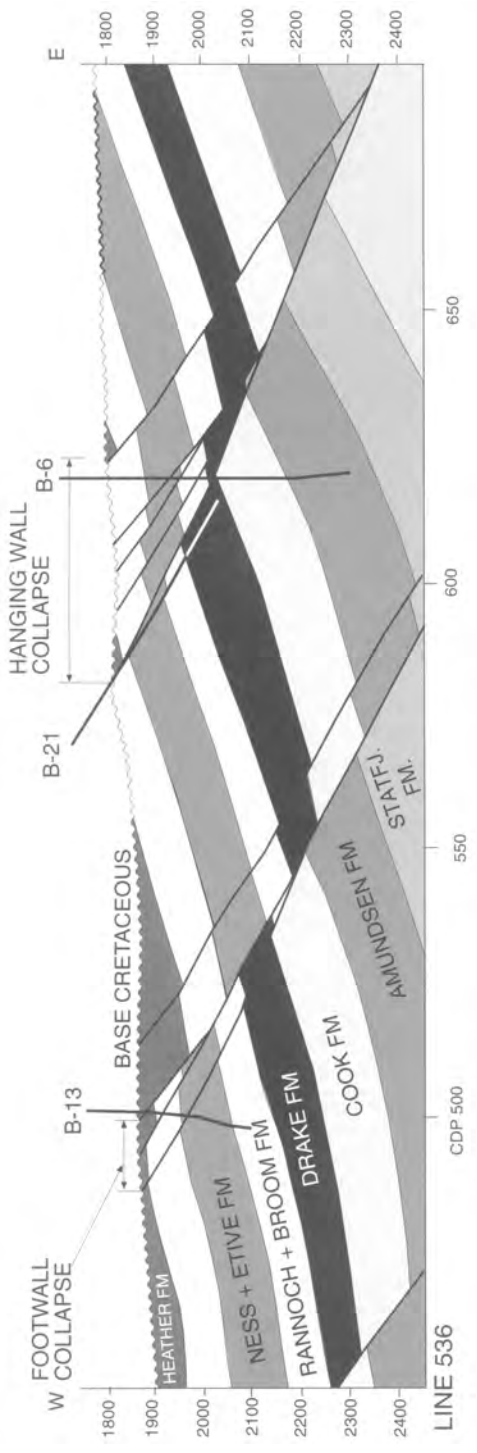

Fig. 7. Profile showing examples of hangingwall and footwall collapse in the domino system.

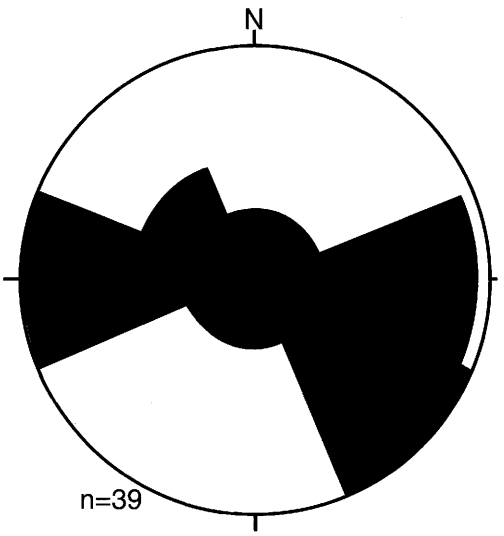

Fig. 8. Rose diagram showing dip directions of faults with associated drag. The diagram shows that N and S-dipping (i.e. E–W-striking) faults have not developed drag structures detectable from dipmeter data.

(Fig. 12). This difference in average dip of about 3.6° indicates a decrease in dip from the Statfjord Formation and upwards through the Brent Group, a difference that locally can be seen directly on the seismic (Fig. 13).

There is a general decrease in dip from the east (footwall position) to the west (hangingwall position) within the domino fault blocks, although variations exist within, as well as between, the blocks. A schematic illustration of the general geometry is given in Fig. 14 (inset). In order to better describe and quantify these changes, the dip of the bedding was plotted with respect to the distance from the nearest main fault to the west. This was done for each fault block defined in Fig. 5 for the top Rannoch and top Statfjord Formations, and the results are given in Table 1.

Figure 14 shows the result of the analysis for fault block B (Fig. 5). A linear regression analysis indicates an average change in dip of 4.6 and 3.6° km^{-1} for the top Rannoch and top Statfjord Formations, respectively. Table 1 shows that the dip gradient generally falls between 1 and 5° km^{-1} in the domino system. This gradient, which is different for the top Statfjord and Rannoch Formations, varies from block to block. The difference in dip gradient between the two horizons is largest in block D (difference of *c.* 2° km^{-1}) and E (difference of *c.* 3.5° km^{-1}), and particularly in block G where the gradients have opposite signs.

A map coded with respect to dip categories of most of the domino area displays the general geometry described above (Fig. 15). This general picture is confirmed by analysis of dipmeter data. Well 34/10-8 is a vertical exploration well located within the domino system in the southern part of the Gullfaks Field. A seismic section through the area (Fig. 16) shows that the uppermost part of the well in the reservoir zone is located in the middle of a large fault block. Towards the base, the well penetrates three minor east-dipping faults and approaches, without penetrating, a fourth east-dipping fault with somewhat larger offset (several tens of metres).

Stereonet plots of the different formations penetrated by the well (Fig. 17) show that beds in the Tarbert to Rannoch Formations dip to the west, and dip is clearly decreasing with depth. Beds in the Drake Formation are subhorizontal or dip very gently to the west, whereas in the Cook Formation, beds dip to the east.

Dipmeter data from well 34/10-8 show that it penetrates the axial surface and the crestal surface (the crestal surface joins the position of lines connecting points of minimum dip of successive layers). Since the well is vertical, such an intersection is only possible if the axial and crestal surfaces are inclined. The simplest interpretation is an east-dipping axial surface. This is consistent with folding of strata due to large-scale drag related to the east-dipping main fault recognized from seismic data. This major drag zone may be described as a triangular zone (Fig. 18). The zone is bounded by the main fault to the west and a less well-defined eastern boundary (there may be a gradual transition from the area affected by drag to the area relatively unaffected by drag). Seismic data indicate that the eastern boundary and the dip isogons in the zone have steeper dips than the main fault, and therefore intersect the main fault at depth (usually at the stratigraphic level of the Statfjord Formation or deeper). The triangular drag zone developed in the hangingwall to main faults is a large-scale expression of more deformation of the hangingwall than of the footwall. A similar relationship was found for minor faults (Fig. 9b).

Relationship between strike of faults and bedding

The strike of the bedding is seen from Fig. 19 to be mostly N–S with a slight NE–SW component. Average strike direction from Bingham analysis (Bingham 1964; Cheeney 1983) for the top

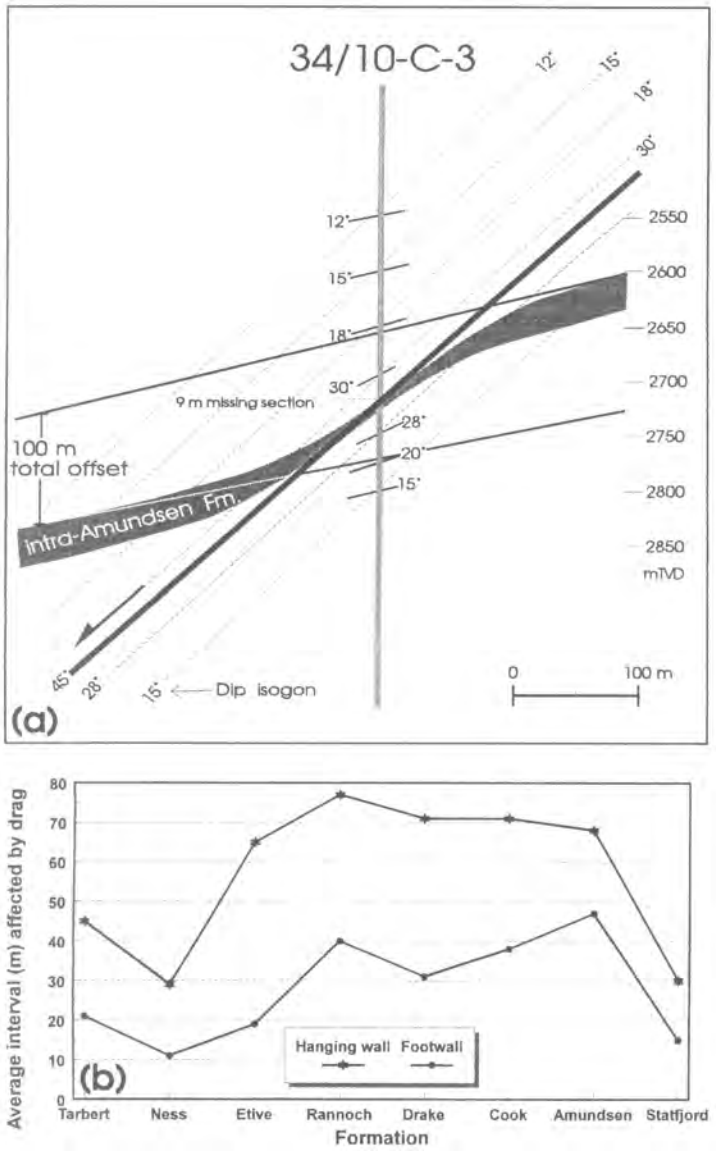

Fig. 9. (**a**) Construction of bedding geometry around a minor fault encountered in well 34/10-C-3, based on detailed dipmeter analysis. There is 9 m of missing section in the well, whereas the total offset across the deformation zone (including local drag deformation) is about 100 m. (**b**) Average interval affected by drag for 46 minor faults in the various Jurassic formations in the Gullfaks Field. The drag zone is wider in the hangingwall than in the footwall.

Rannoch and Statfjord Formations are 009 and 006, respectively. Ideally, the strike of the bedding and the faults would be expected to be parallel in a simple domino system. However, the faults show an average strike that is slightly west of north, with a maximum around 350 (Fig. 20). This difference in strike of 15–20° can also be seen on the contour maps, particularly in blocks D–F where the contour lines can be traced southwards from the eastern side of the fault block to the western side (Fig. 4). An explanation for this discrepancy is that the rotation of the layers in the Gullfaks area was not solely controlled by the domino faults within the Gullfaks

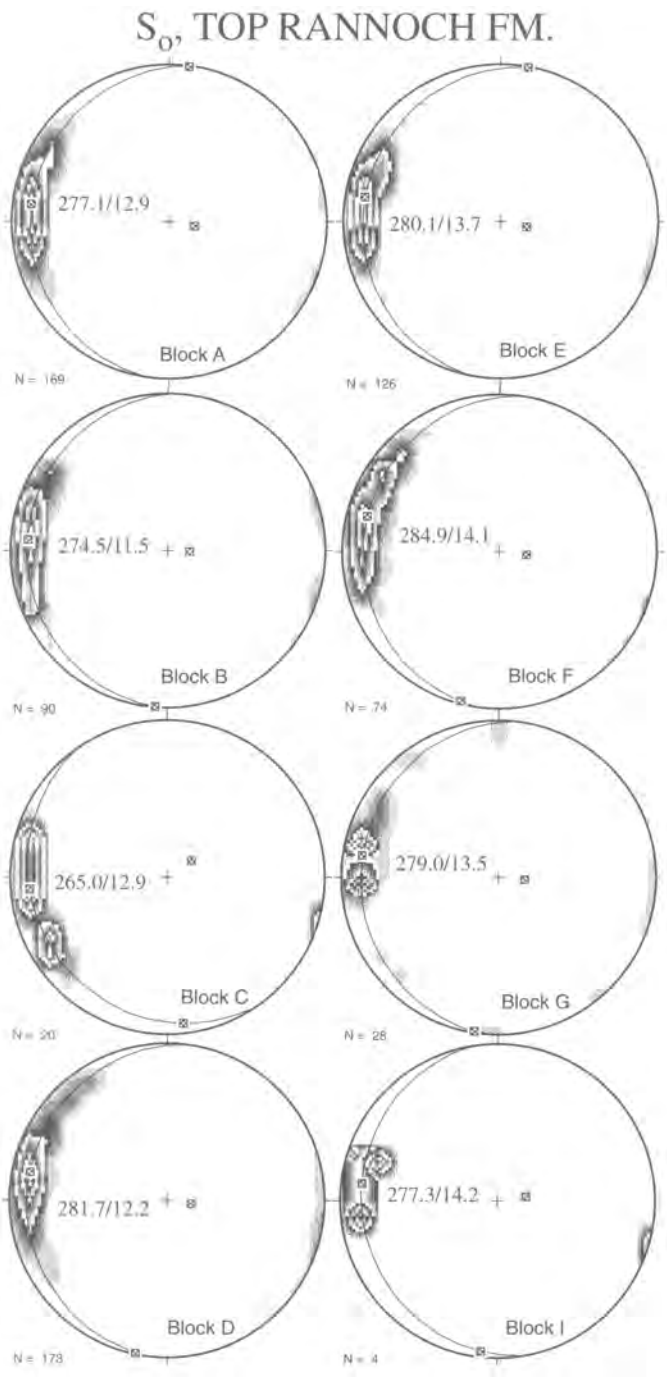

Fig. 10. Dip azimuth/dip of bedding plots for the top Rannoch Formation. Block numbers correspond to domino blocks labelled in Fig. 5.

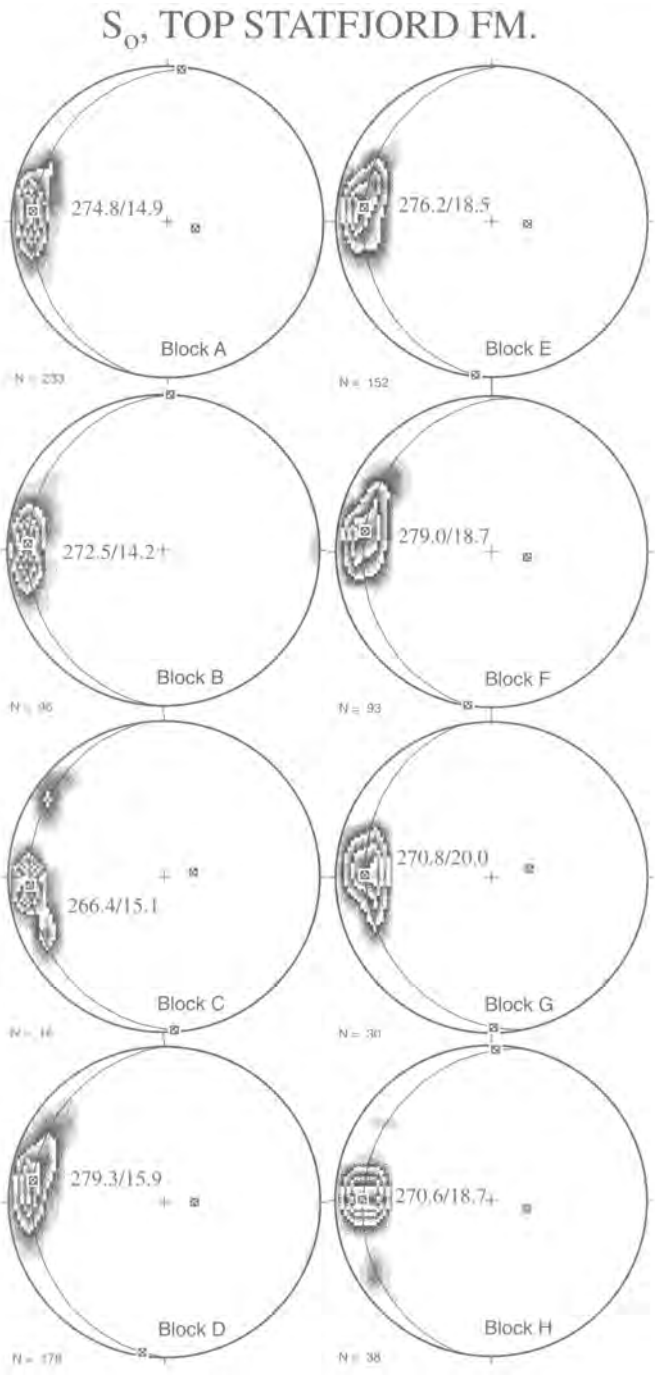

Fig. 11. Same as Fig. 10, but for the top Statfjord Formation.

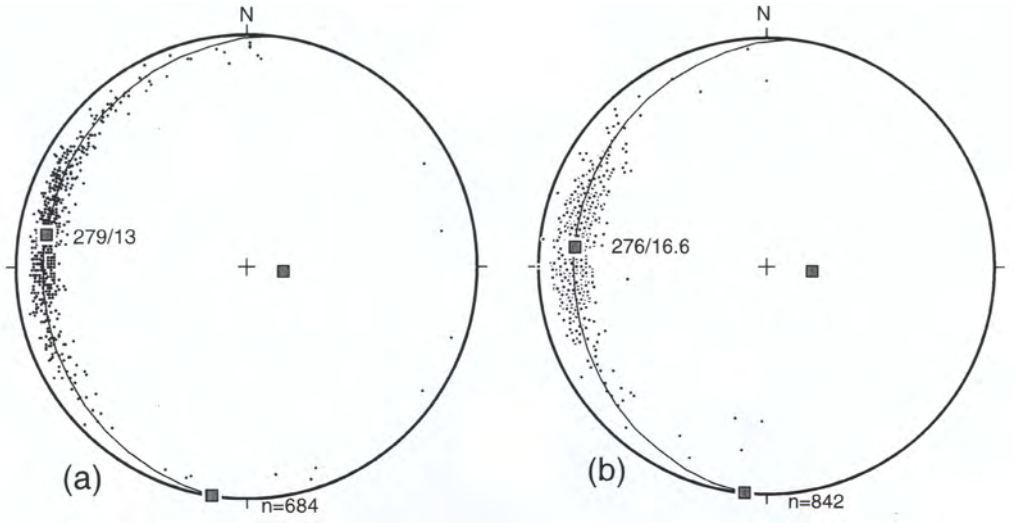

Fig. 12. Dip azimuth/dip plots of bedding from the domino area for (**a**) the top Rannoch Formation, and (**b**) the top Statfjord Formation.

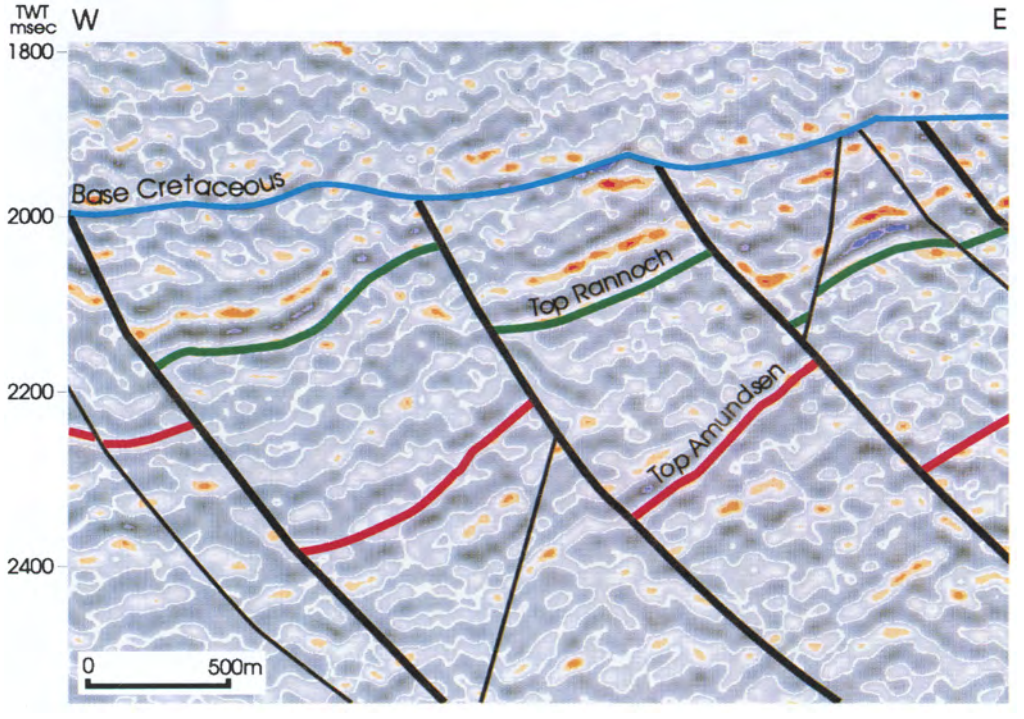

Fig. 13. Seismic line showing difference in dip between the Brent Group and the Statfjord Formation.

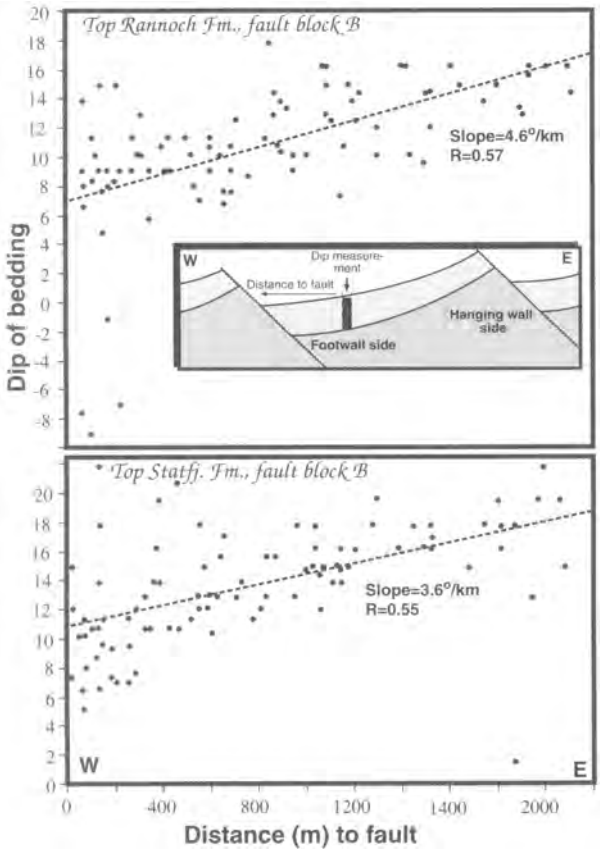

Fig. 14. Dip–distance plot for the top Statfjord and the top Rannoch Formations, fault block B (see Fig. 5 for location). The data indicate a general geometry similar to the one shown in the inset sketch, i.e. steepening bedding to the east across the fault block.

Table 1. *Statistical dip versus distance data for domino blocks defined in Fig. 5*

	Rannoch Fm.				Statfjord Fm.		
Block	Grad (°/km)	*R*	*n*	Block	Grad (°/km)	*R*	*n*
B	4.58	0.567	90	B	3.58	0.550	90
C	(2.13)	0.182	20	C	(5.5)	0.412	20
D	4.67	0.371	173	D	2.64	0.243	173
E	6.61	0.515	126	E	3.13	0.300	126
F	3.21	0.307	74	F	2.6	0.315	74
G	8.05	0.351	28	G	−7.04	0.522	28

With the exception of block C, all the listed fault blocks contain data that conform to significant linear correlations for a chosen risk of error of 5%. *R*, coefficient of linear correlation; *n*, number of observations.

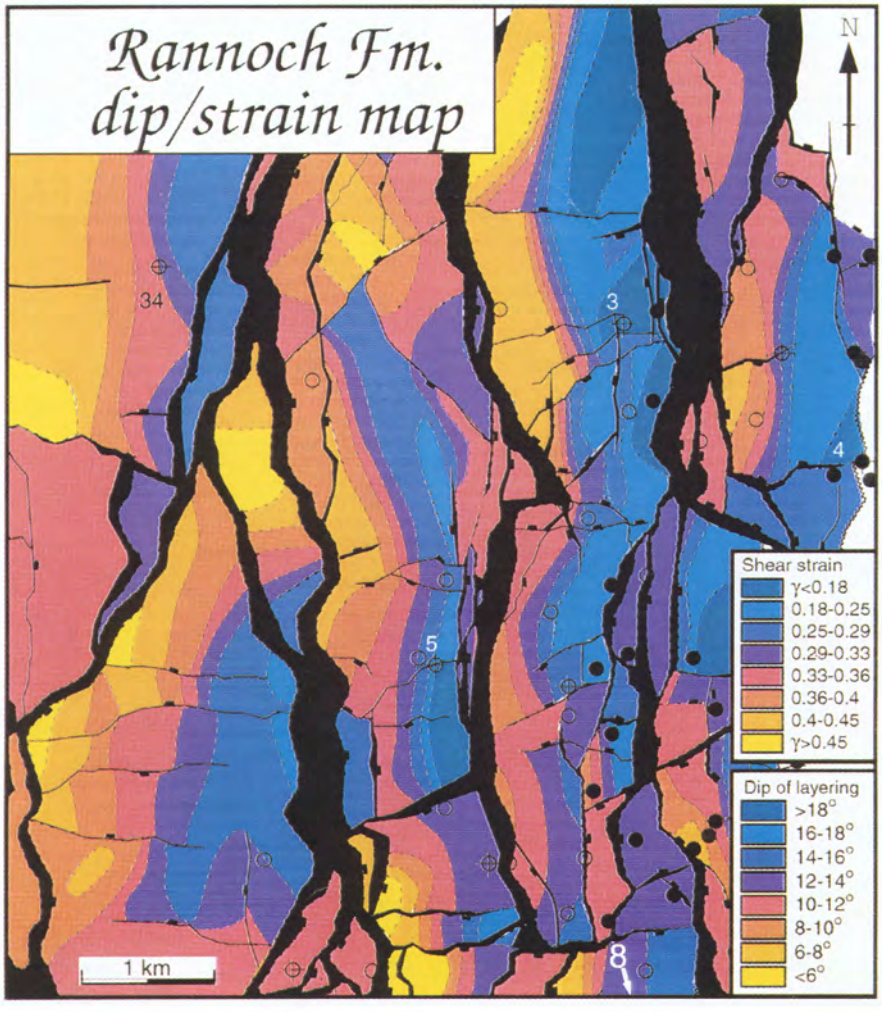

Fig. 15. Colour-coded dip map for the main part of the domino area. The general steepening bedding to the east across domino fault blocks is seen across the area. An additional code indicates shear strain according to the relationship between bedding and shear strain indicated in Eqn 8.

Field, but also by the more NNE–SSW-trending, first-order faults separating the Gullfaks fault block from the Statfjord Field (Fig. 1). The strike of the bedding falls somewhere between the strike of the first- and second-order faults, and may thus have been affected by rotation related to both sets of faults.

The eastern horst complex

Geometry of faults

The main faults in the horst complex are considerably steeper than those in the domino area. Dips of about 60–70° are common, and both E- and W-dipping faults occur (Fig. 20a). A very constant N–S strike is characteristic for the main faults, and these faults are more planar than the main faults in the domino system to the west.

The Jurassic sediments that generate good reflectors in the main part of the Gullfaks Field are eroded in the horst complex. This makes mapping of minor faults more uncertain in the horst complex. Most mapped minor faults are relatively steep (45–70°) and run sub-parallel to the main faults.

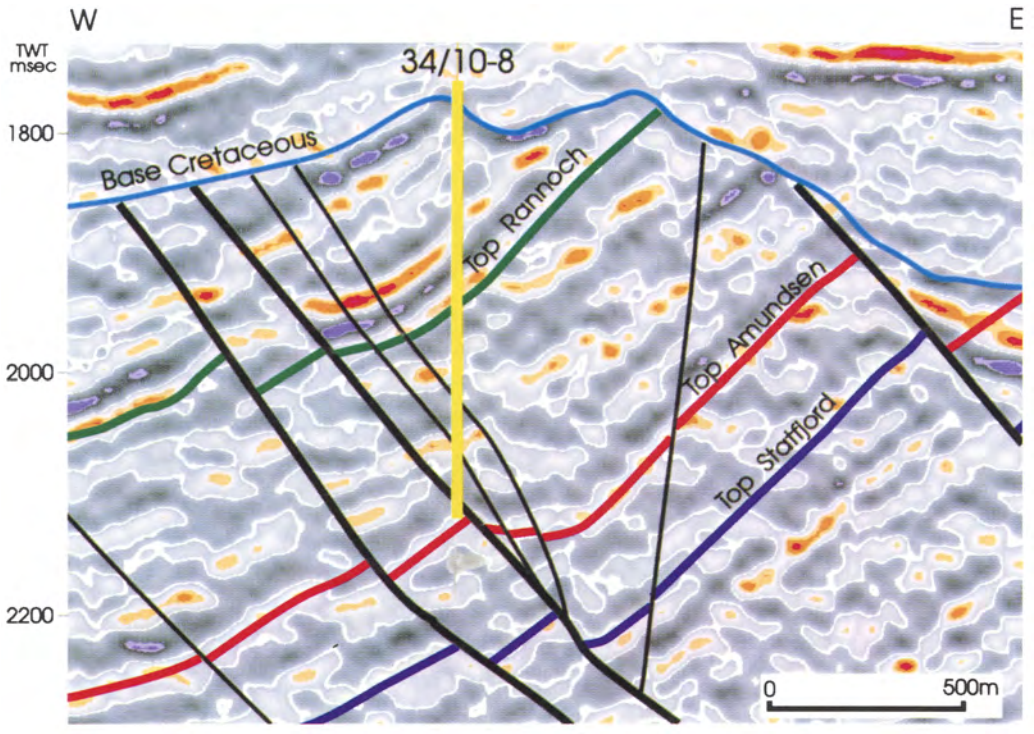

Fig. 16. Seismic line through well 34/10-8. Note pronounced flattening of beds in the western parts of the fault blocks (large-scale drag).

Geometry of bedding

The bedding in the horst complex is sub-horizontal with a weakly preferred westerly dip direction. A perturbation of the bedding is seen in the northern part of this area (around well 34/10-C-2) where a doubly plunging fold with shallowly plunging, NW–SE-trending axial trace and steep axial surface has been mapped.

Dipmeter data from the horst complex support the seismic interpretation, suggesting sub-horizontal dips or shallow dips to the west or to the south.

The transitional accommodation zone

The zone between the domino system and the horst complex accommodates the difference in structural style between the two areas, particularly the difference in dip of bedding and faults on either side of the zone. The accommodation zone is a graben structure, and the bedding defines a fold with a W-dipping western limb and a sub-horizontal to gently E-dipping eastern limb.

Fault geometry

The main faults associated with the accommodation zone are the easternmost domino fault, i.e. a relatively low-angle (25–30°) fault, and the steeper (65°) W-dipping fault bounding the horst complex to the east. Minor faults show a preference of N–S and E–W strikes with variable dip (Fig. 20b). Physical modelling suggests that this is an area of many small faults of which we have been able to identify only a small fraction (Fig. 21).

Geometry of bedding

The bedding in this zone defines a somewhat modified (faulted) fold with a western limb that dips about 15° to the west, and an eastern, gently E- to ENE-dipping limb. The axial trace of the fold trends approximately NNW–SSE, and the fold axis plunges very gently to the NNW. From the measured poles to bedding at Cook level in the fold area, the fold axis was estimated to be oriented at 345/06 (Fig. 22a). The opening angle of the fold is *c.* 160°, and the axial plane appears to be steep.

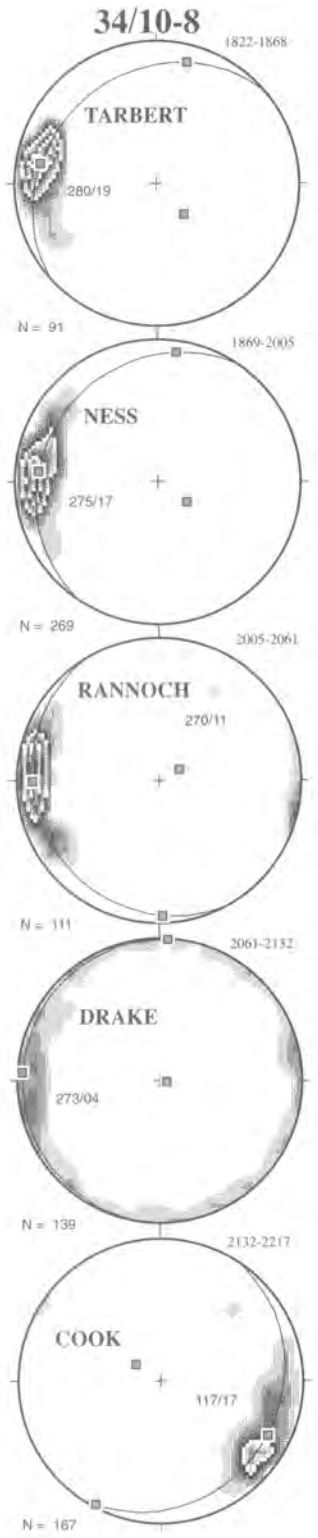

Well 34/10-C-1 is located within the accommodation zone (Fig. 4). The well is drilled in a southwesterly direction and penetrates the eastern limb, the axial surface, and the western limb of a seismically defined gentle fold (Fig. 23). The fold displays a slightly east-dipping eastern limb, and a more steeply dipping western limb. Dipmeter data from this well show relatively shallow easterly dips in the uppermost strata in the reservoir zone (eastern limb) (Fig. 24). Subhorizontal dips dominate in the hinge zone, changing to gradually steeper (up to 22°) westerly dips as one enters the western limb. The intersection between the axial surface of the fold and the well is interpreted to be within the Statfjord Formation. Plotting the maximum concentration of poles to bedding from the two limbs gives a sub-horizontal fold axis with a southerly trend (176/01, Fig. 22b).

The effect of compaction

Compaction leads to a reduction in both dip and length of non-horizontal and non-vertical faults and beds. The angular changes involved can be expressed by the simple trigonometric relationship:

$$\theta = \tan^{-1}[(1 + \Delta)\tan\theta_0] \qquad (1)$$

where θ and θ_0 are the present and initial dips of the fault in question. The present fault dip is normally known and, assuming a compaction factor Δ, one wants to calculate the initial dip of the fault. Equation 1 can then be rewritten as:

$$\theta_0 = \tan^{-1}[\tan\theta/(1 + \Delta)] \qquad (2)$$

On the Gullfaks Field, the main faulting initiated during, or immediately after, the deposition of the Tarbert Formation, i.e. the top of the Brent Group was at the surface at the time of faulting. The fault surfaces were deformed by the subsequent compaction history of the sediments, which mainly occurred while the structure was buried in Late Cretaceous time and overlain by some 2 km of mostly Tertiary sediments. Near-sea bottom measurements of sand porosity generally fall within 38–43% (Perrier & Quiblier 1974), although the porosity is quickly reduced during burial. Hence, we can assume the original porosity of the sandy intervals of the Brent

Fig. 17. Stereographic projections of dipmeter data (dip azimuth/dip of bedding measurements) from well 34/10-8. A change from westerly dipping beds in the upper part of the well to easterly dips in the lower part confirms the seismic expression seen in Fig. 16.

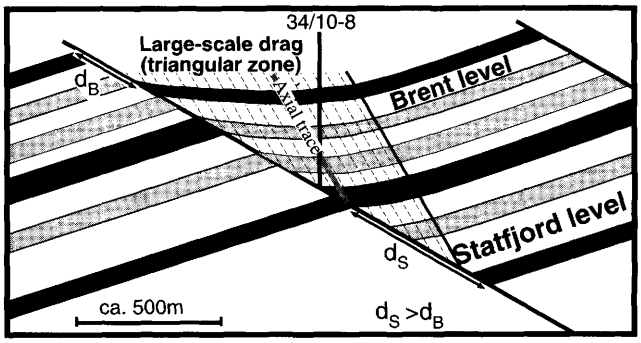

Fig. 18. A generalized section through a domino block, showing the triangle-shaped large-scale drag zone. The displacement at deeper reservoir levels (d_S) is larger than at higher levels (d_B) due to the dissipation of deformation upwards into the hangingwall. The principal location of well 34/10-8 is indicated.

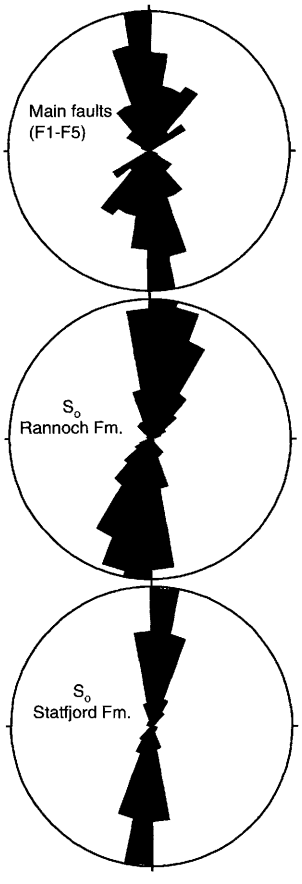

Fig. 19. Orientation (strike) of main faults and bedding (Rannoch and Statfjord Formations) in the domino system, Gullfaks. A difference of about 10–20° between the fault orientations and the bedding is evident from the rose diagrams. See text for discussion.

Group to have been around 40% ($\phi_0 = 0.4$). Shale, on the other hand, has a considerably higher initial porosity (85–50% within the upper 10 m of a clay sequence), but decreases rapidly with depth.

The present porosity of the oil-filled sandstones of the Brent Group varies from $\phi = 0.2$–0.34 with a maximum close to 0.3. Their porosity can therefore be assumed to have changed from about 40% near sea-bottom to the present 30%. For $\theta = 0.3$, using the relationship

$$\Delta = [(1 - \phi_0)/(1 - \phi)] - 1 \qquad (3)$$

which yields $\Delta = -0.14$ (i.e. 14% vertical shortening).

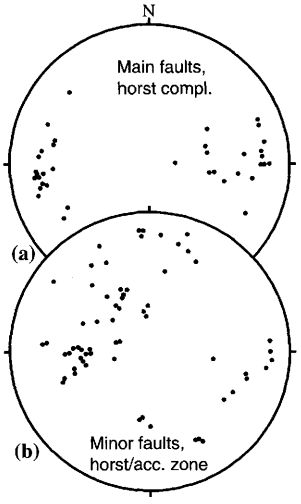

Fig. 20. (**a**) Poles to major faults in the horst complex, (**b**) minor faults in the accommodation zone and horst complex.

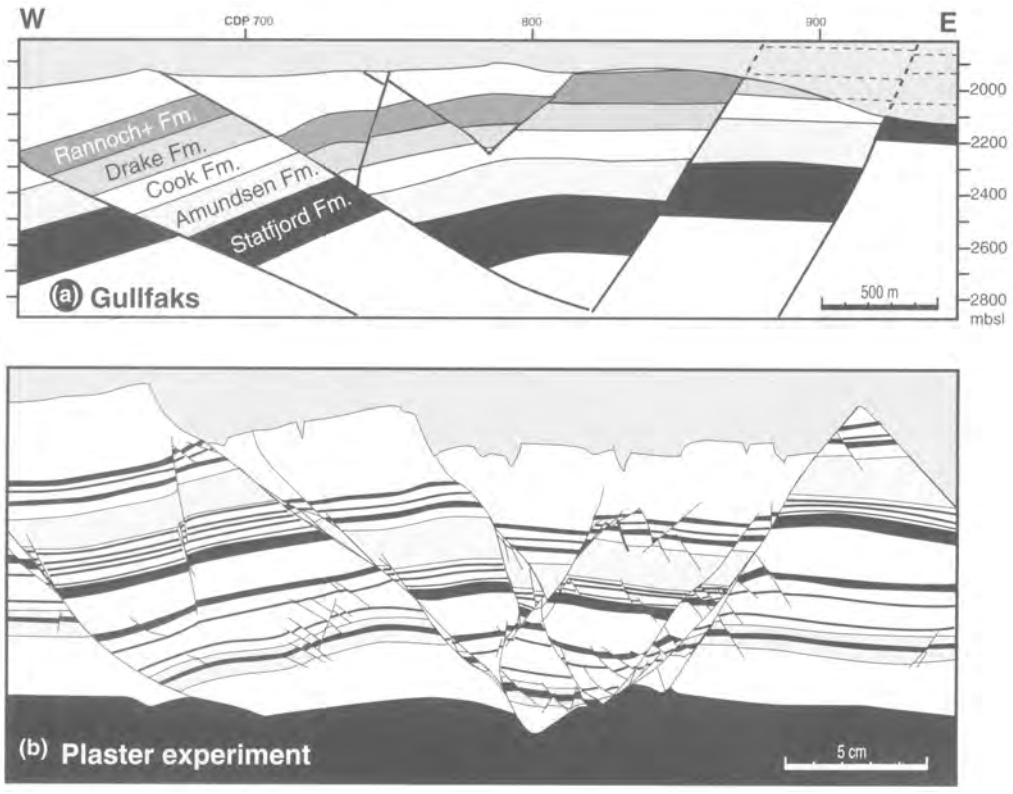

Fig. 21. (**a**) Seismic line (912) across the accommodation zone, showing a gently collapsed fold structure. (**b**) Part of plaster model (detailed part of experiment shown in Fossen & Gabrielsen (1996)), showing a remarkably similar geometry to (a), but with a large amount of additional small-scale faults and fractures.

The Brent Group consists of *c.* 77% sand, of which the upper and lower 100 m contain 90% sand and the middle part (Ness Formation) about 50% sand. For pure sandstones, faults with present dips of 25–30° (Fig. 6) in the uppermost part of the Brent Group would have had pre-compactional dips of 28.5–33.9° according to the numbers above (Eqn 2). Hence, it can be concluded that the lowering of fault dips due to compaction may be in the order of 4° for the uppermost part of the Brent Group, decreasing downwards through the reservoir.

Shales of the Ness Formation were buried to depths of 100–200 m during faulting. Considerable dewatering (compaction) had therefore already taken place prior to faulting. The subsequent reduction in porosity is assumed to be quite similar to the adjacent sandstones. The effect of this type of compaction history on initially planar faults is to form slightly convex-upward or 'anti-listric' fault geometries in the upper part of the reservoir because of the decreasing effect of post-faulting compaction with depth. Alternatively, if the fault had a gently listric initial geometry, it has been straightened out during the post-faulting compaction history.

In addition to the effect on fault geometry, compaction would also influence the orientation of the bedding. For layers now dipping at 12–14° (Rannoch Formation, Fig. 10), a change in porosity from $\phi_0 = 0.4$ to $\phi_0 = 0.3$ gives a pre-compactional dip of 14–16°. Hence compaction may have lowered the dip of the bedding by an amount of *c.* 2.4° in the uppermost part of the Brent Group, rapidly decreasing downwards. Hence, the post-tectonic dip is unlikely to have changed significantly during the post-rift burial history of the pre-Tarbert Formation section, and the difference in average dip between the Rannoch and Statfjord Formations indicated in Fig. 12 is largely caused by tectonic deformation.

Vertical changes in post-faulting compaction could in principle give rise to large-scale drag or hangingwall synclines of the type shown in Fig. 18, but modelling shows that this effect is negligible on Gullfaks.

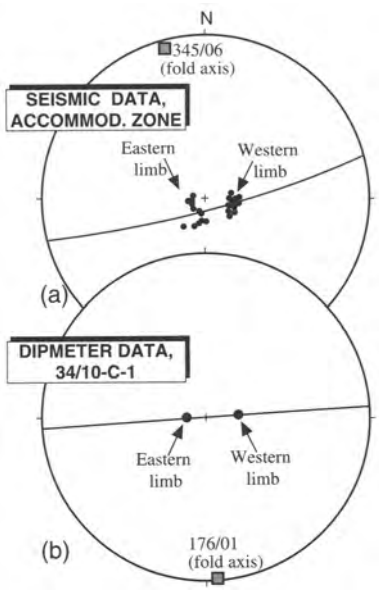

Fig. 22. (**a**) Poles to bedding in the accommodation zone/fold area from seismic interpretation, and (**b**) maximum concentrations of bedding from dipmeter data in well 34/10-C1. In both cases, an almost N–S-trending sub-horizontal fold axis is indicated.

Fault geometry, forward modelling and internal block deformation

Initial fault dips

One of the puzzling features of the Gullfaks Field is the anomalously low dips of the fault planes in the domino area, compared to the low dips of the sedimentary layers and to the moderate amount of regional Jurassic extension. In general, the well-known Navier–Coulomb criterion for brittle failure can be expressed as:

$$\tau = C + \sigma_n \mu \qquad (4)$$

where τ and σ_n are the shear and normal stresses, respectively, acting on the potential fracture plane, and μ is the coefficient of internal friction ($\mu = \tan \eta$, where η is the angle of sliding friction). C is the cohesion or inherent shear strength of the rock. From this criterion, the angle φ between the shear plane (fault) and the axis of maximum principal stress (σ_1) can be predicted to be:

$$\varphi = \pm(45° - \eta/2) \qquad (5)$$

(e.g. Price & Cosgrove 1990). During extensional deformation σ_1 is vertical, and the initial dip

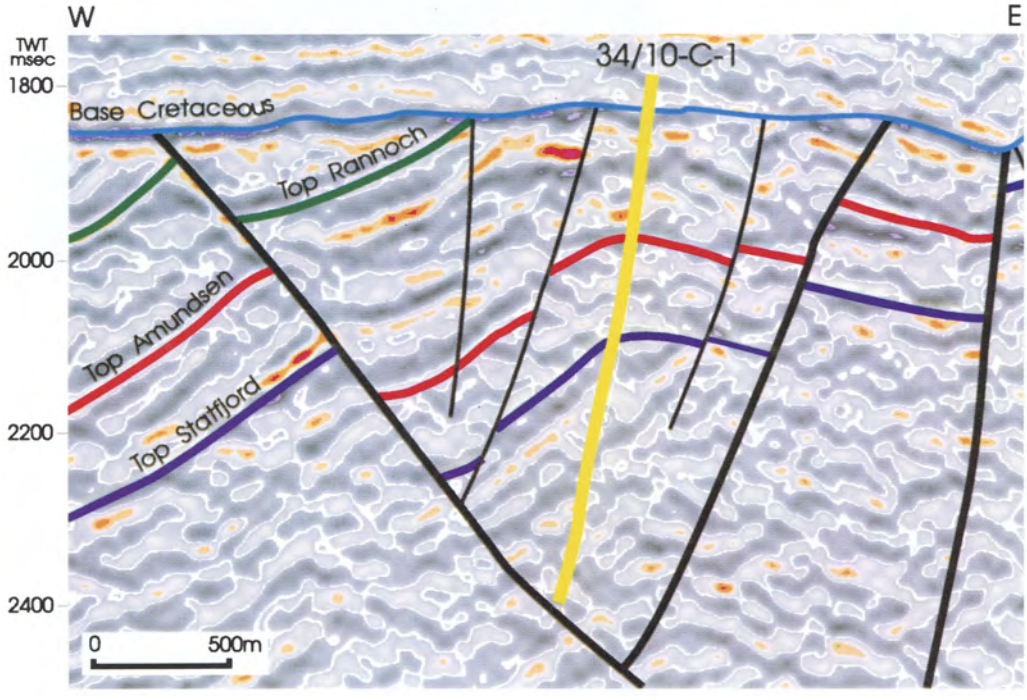

Fig. 23. Seismic line through well 34/10-C-1. According to the seismic interpretation, the well penetrates the fold in the accommodation zone.

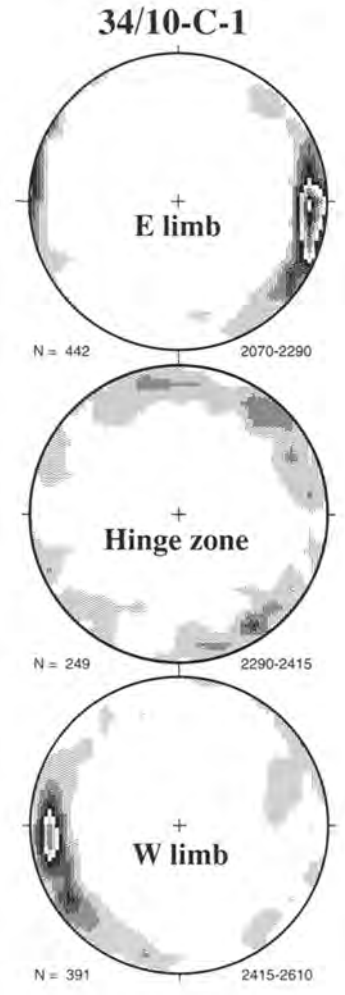

Fig. 24. Dipmeter data (dip azimuth/dip) from well 34/10-C-1 from what is interpreted as the east limb, the hinge zone and the west limb according to the seismic interpretation (see Fig. 23). The dipmeter data support the seismic interpretation.

($\theta_0 = 90 - \varphi$) of a normal fault will be higher than 45° by an amount depending on η. Based on studies of fault-plane solution data, Jackson (1987) argued that θ_0 is typically about 60°, as suggested by Anderson (1951). Walsh & Watterson (1988), on the other hand, presented fault dip measurements from British Coalfields, and found that the mean dip of normal faults is about 70° rather than the commonly accepted value of 60°. They also refer to several studies where the mean dip angle is, or is inferred to have initiated at values between 60 and 75°. Their data were collected from consolidated rocks (depth of faulting is 2–3 km), except for four syn-sedimentary faults which exhibited lower dips. However, faults in poorly consolidated sands and conglomerates also exhibit fault dips in the order of 60–70° in many extensional settings, e.g. in the Lake Havasu/Whipple Mountains area of Arizona/California (unpublished data) and in sandbox experiments, and the existing data therefore do not suggest a significantly shallower angle of faulting in poorly consolidated sediments.

Initial fault dips on Gullfaks

The main faults in the Gullfaks Field formed in mostly consolidated rocks, and only the uppermost part of the fault planes affected what was poorly consolidated sediments at the time of faulting. The dip of the Gullfaks faults was estimated at Statfjord level (at 800–1000 m depth during faulting), and fault dips remain constant at least into the Teist Formation some 1–2 km further down (Fig. 1, profile). According to the discussion above, one would expect initial fault dips in the order of 60–70°.

The present dip of the main faults in the horst complex on the Gullfaks Field is found to be about 60–65°. The effect of post-faulting compaction must have been small in the Triassic–Lower Jurassic layers, and even in the Brent Group it cannot have changed the fault dip by much more than 4° (see discussion above). Also, a very gentle westward tilting of the horst complex counteracts the effect of compaction. The initial dip of the faults in this area must therefore have been about 60–70°. Given the fact that there is no difference in the lithological or mechanical properties of the sediments in the horst and domino area, it is likely that this was also the initial dip of the faults in the domino area, i.e. that the main faults in both the domino area and the horst area started out with approximately the same dip. Otherwise, the maximum principal stress (σ_1) must have deviated considerably from vertical over a very short distance, an unlikely situation on this scale in an extensional rift setting. Furthermore, the change from steep faults in the horst area to low-angle faults in the domino area is closely associated with a change from flat to inclined bedding. This closely associated change in fault and bed geometry occurs rapidly across the accommodation zone, and suggests that the change in fault dip is not an initial feature, but rather is related to rotation and internal block deformation.

The domino faults of the Gullfaks Field appear to be rooted in a low-angle detachment fault (Fossen *et al.* in press), and thus occur in

the upper plate of a detachment system. Upper plate faults typically initiate as high-angle faults that correspond well with mechanical models of fault initiation. Hence, there is no reason to expect that the main faults in the domino area on Gullfaks should not have originated as high-angle normal faults. Based on the discussion above, we will in the rest of this paper assume that all the main faults initiated with 60–70° dips. It is emphasized that the alternative model, where the faults in the domino area originated at considerably lower angles, would change some of the results presented below.

The rigid domino model

The (rigid) domino or bookshelf model (e.g. Jackson 1987; Mandl 1987; Axen 1988; Davison 1989) is the simplest model that explains the development of sub-rectangular fault blocks separated by straight faults in a cross-section. The main assumption is that the fault blocks, and therefore also the associated faults, rotate rigidly during deformation. No internal deformation takes place within the domino blocks in this model. This implies that the cut-off angle between the faults and the layers remains constant throughout deformation, and both bedding and faults will rotate at the same rate and by the same amount. If α is the dip of the bedding and θ is the dip of the fault plane, then the initial dip of the fault (θ_0) is simply:

$$\theta_0 = \theta + \alpha \qquad (6)$$

For the Gullfaks domino area $\alpha \approx 15°$ (average pre-compactional dip, Rannoch Formation), and $\theta \approx 30°$ for the main faults. The rigid domino model thus gives $\theta_0 = 45°$, which from the discussion above is unrealistically low. Similarly, if the main faults in the domino area initiated with dips of about 65°, their present dips (25–30°) indicate a rotation of the faults in the order of 35° (anti-clockwise when looking north). This contrasts to the rotation of the bedding in the domino area, which is about 15°. From this, and from the fact that bedding is not planar, it can be concluded that the rigid domino model does not work satisfactorily for the main, western part of the Gullfaks Field (see also Koestler *et al.* 1992).

The soft domino model

The soft domino model is similar to the rigid domino model except that it allows for additional internal deformation of fault blocks. Simple models describe internal deformation as distributed (homogeneous or heterogeneous) vertical shear (Westaway & Kusznir 1993), inclined shear synthetic or antithetic to the domino faults (e.g. White *et al.* 1986) or layer-parallel slip (a special case of inclined shear) (e.g. Higgs *et al.* 1991).

A general E–W section through the Gullfaks Field was constructed for forward modelling purposes (Fig. 25). Starting with the domino area, we assume from the discussion above that the initial angle of faulting was everywhere 60°. Applying 30% extension (more in the domino area and less in the horst complex) (Fig. 25b) and vertical movements leads to Fig. 25c. The geometry in the horst complex is already similar to the Gullfaks horst complex geometry, and neither block rotation nor internal deformation is required here.

The domino area, however, needs rotation after stage (c) in Fig. 25. This results in either steeply (30°) W-dipping bedding (as shown in Fig. 25d), or steeply (55°) E-dipping faults if bedding is balanced. Some additional deformation must therefore be applied to achieve the observed geometry, for example a combination of rigid rotation and inclined shear parallel (synthetic) to the main faults (Fig. 25e). This model is, however, only one of many possible deformations that could lead to the desired geometric relationships. Fault-parallel shear (Fig. 26b), antithetic shear alone (Fig. 26c), or a combination of rigid rotation and layer-parallel (antithetic) shear as in Fig. 26d can lead to exactly the same angular relationship. Vertical shear, on the other hand, cannot produce the desired geometry (Fig. 26e).

To assess this problem, it is necessary to take into account the non-planar geometry of bedding within the domino blocks. Dips of bedding up to 25° are mapped in the footwall to faults, which by rigid body rotation would give initial fault dips of 55°. Little internal deformation is therefore required here if the faults initiated with angles of 60–70°. In the hangingwall parts of the blocks, bedding typically approaches horizontal and the cut-off angle thus approaches 30°. This demonstrates that there is an increasing amount of internal deformation from the east to the west within the domino blocks, i.e. the domino faults separate areas of different strain intensities and thus represent strain discontinuities in the domino system.

The synthetic shear model can be modified to account for the non-planar bedding geometry. To model the observed low-dip triangle zone in the hangingwall to the domino faults, the shear plane must be steeper than the finite dip of the

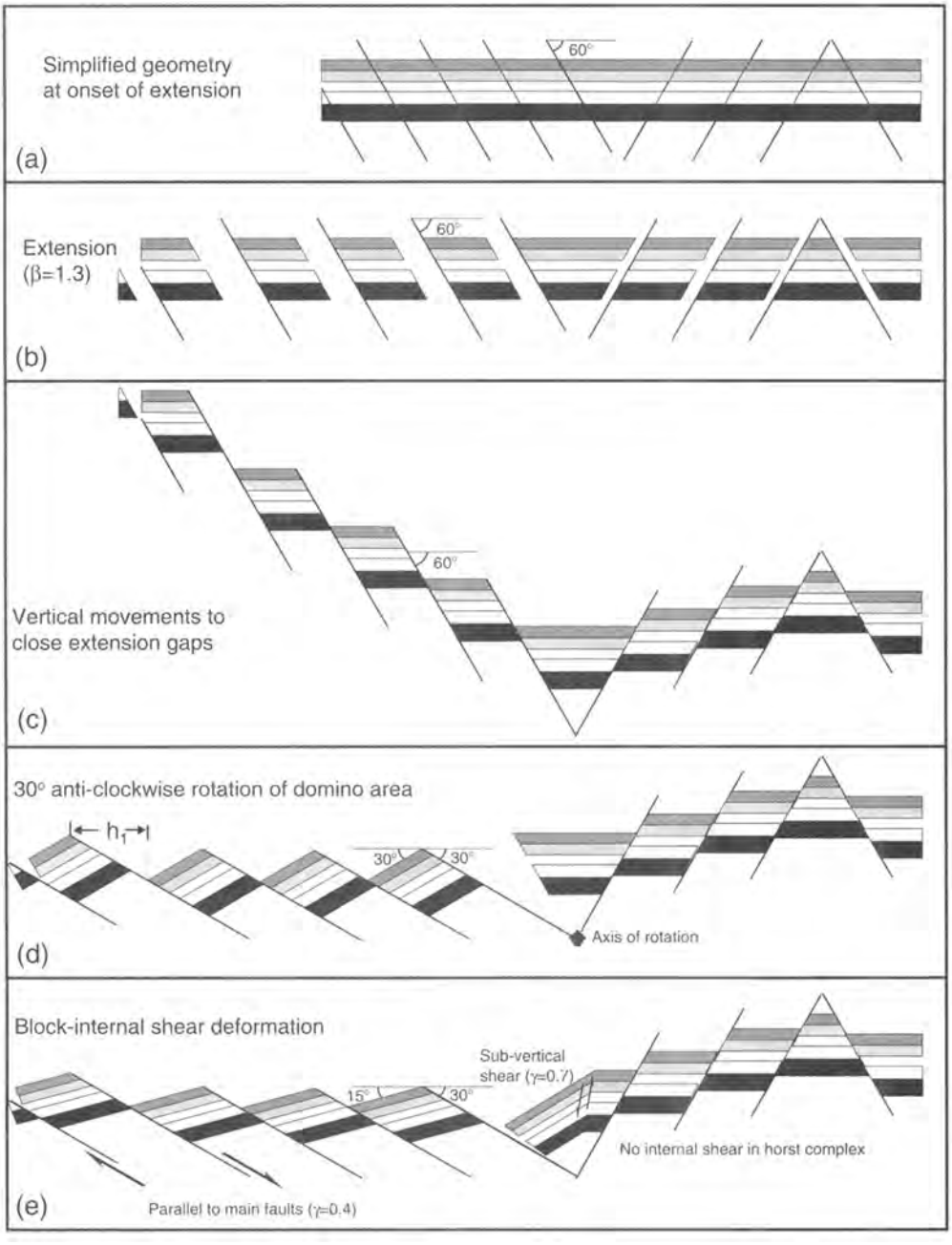

Fig. 25. Forward modelling of the Gullfaks Field by use of a generalized E–W section. (**a**) Initial fault dips are chosen to be 60°. (**b**) Application of 30% extension. (**c**) vertical movements to fill the evolving gaps. Note that the horst complex is adequately modelled at this point. (**d**) Rotation of the domino system so that a 30° dip of the domino faults is achieved. The bedding is now dipping steeply to the left (west), and some internal block deformation must be applied. (**e**) Application of fault-parallel shear gives the wanted dip of the bedding. Similarly, steep W-dipping shear in the accommodation zone helps fill the open gap between the horst complex and the domino system.

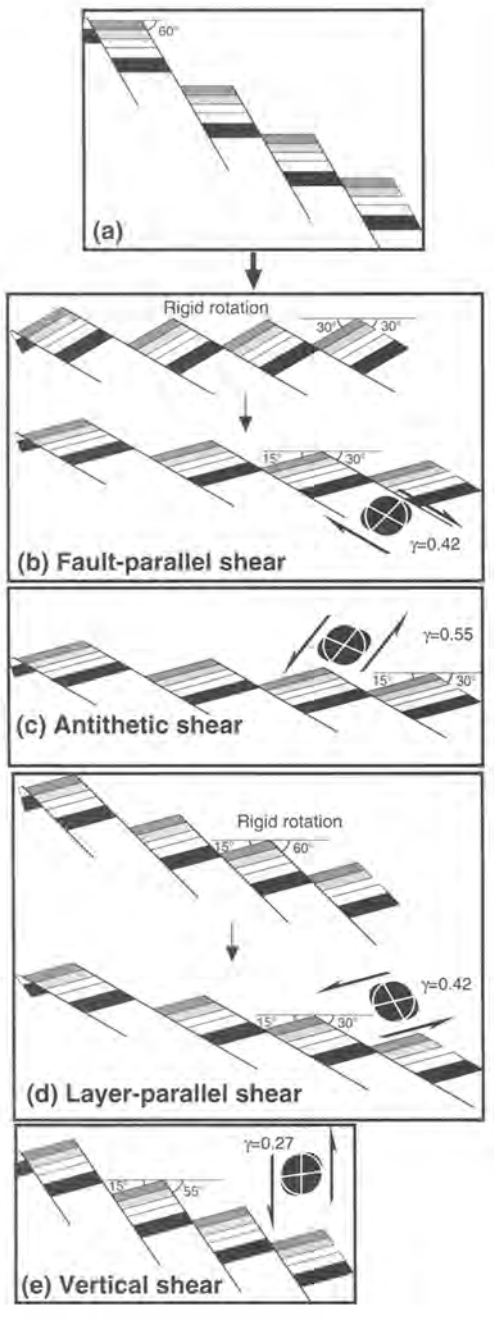

Fig. 26. (**a**) Going from stage (c) in the domino area in Fig. 25, one can end up with faults dipping 30° and bedding dipping 15° not only by fault-parallel (synthetic) shear (**b**), but also by antithetic shear (**c**) or by rigid rotation + bedding-parallel shear (**d**). Vertical shear (**e**) can never produce the observed angular relationship between faults and bedding.

faults (Fig. 27b). Because this simple shear model elegantly explains both the geometry of the bedding and the angular relationship between the faults and the bedding in a simple way, it is accepted as a realistic model for the internal block deformation in the domino area. It also bears geometrical similarities with the model presented by Roberts & Yielding (1993, p. 240).

In contrast, the antithetic shear model predicts a positive relationship between dip of bedding and shear strain (Fig. 27c, d). Hence, for the geometry indicated in Fig. 27a, there must be a triangle in the western and upper part of the block that is unsheared or less sheared than the eastern part. However, this implies compatibility problems if one wants to create the observed abrupt change in dip across the domino faults (open void in Fig. 27d). Compatibility can be maintained by a banded shear model, but faults then become highly non-planar, and bedding geometries at deeper parts of the reservoir do not conform with the actual observations (Fig. 27c). A simple antithetic shear model can therefore be rejected.

The horst complex and the accommodation zone

We assume that the horst and the domino area on the Gullfaks Field formed and deformed more or less simultaneously, and that the main faults were established at an early stage of the extensional history. The relatively flat bedding in the horst complex indicates that this area did not experience any finite rotation during the following extension, i.e. no internal deformation is geometrically necessary (Fig. 25c). An open gap evolves as the domino area undergoes anticlockwise rotation in Fig. 25d, and the area between the horst complex and the domino system must somehow collapse to accommodate this development. This collapse could be modelled by sub-vertical (steeply west-dipping) shear, as indicated in Fig. 25e. However, there is also some evidence (seismic and well data) for a conjugate set of faults that is more pronounced in the upper part of the accommodation zone (Fig. 21a). Plaster experiments (Fig. 21b) indicate that this fault pattern is feasible, but that there is a significant amount of small-scale deformation that is not incorporated in the present interpretation.

Expressions of the internal block deformation

The deformation within the fault blocks on the Gullfaks Field can be sub-divided into minor

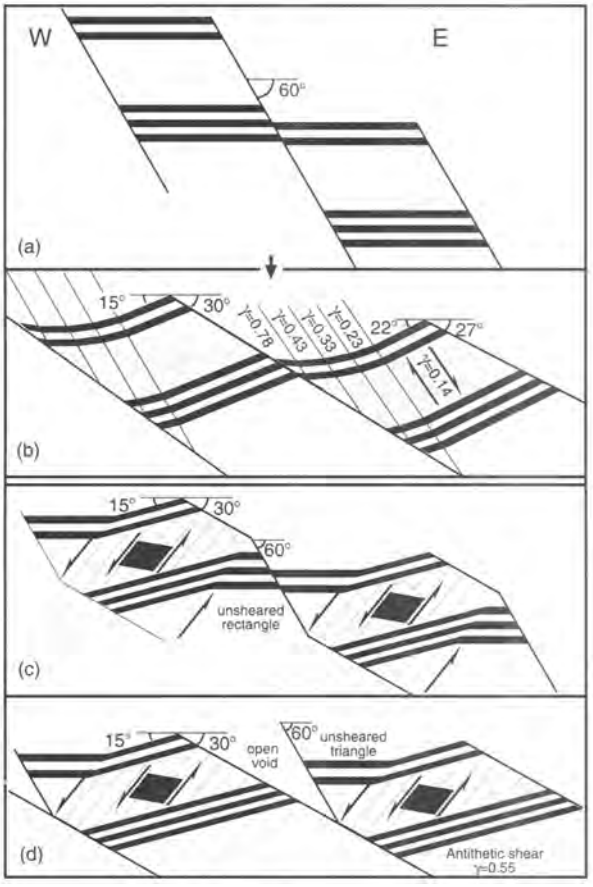

Fig. 27. Forward modelling, taking into account the non-planar geometry of the bedding revealed in this study. (**a**) Horizontal bedding offset by faults dipping 60°. (**b**) A synthetic shear model, where the shear plane is steeper (60°) than the domino faults (30°), produces the desired geometric properties. (**c**) A banded antithetic shear model provides strain compatibility, but the geometry of faults and bedding in the deeper parts of the sequence does not confirm the geometric data from the Gullfaks domino area. (**d**) Antithetic shear, leaving a triangle in the hangingwall unsheared to obtain the low-dip triangle zone. Note the resulting open void.

faults (seismically resolvable), sub-seismic (discrete) fractures, and continuous ('ductile') deformation (Fig. 28). A statistical fault population study (Fossen & Rørnes 1996) shows that the total seismically resolvable fault population is not fractal, and that a segmented throw population curve exists in log–log space within the range of seismic resolution. However, minor faults define sub-populations that follow exponential scaling laws, although it is uncertain if these laws can be extended into the sub-seismic domain.

The geometries and spatial distribution of sub-seismic faults are hard to predict. Comparing the orientation of the main faults with the seismically resolvable minor faults (Figs 3 and 4) reveals a significant difference in orientation, and sub-seismic faults may or may not reflect the orientations of either large or small seismically resolvable faults.

As an example of the difficulties involved in predicting sub-seismic fault orientation, we refer to a recent study of fault block B (see Fig. 5). The sub-seismic (1–50 m displacement) fault pattern was modelled numerically (Fig. 29a), based on quantitative data from an onshore field area (Koestler *et al.* 1994) and assuming that sub-seismic faults are more or less parallel to the seismic faults. The modelling was based on an old (1987) seismic interpretation of the block. The seismic data resolution has since been improved by reprocessing, and seismic attribute

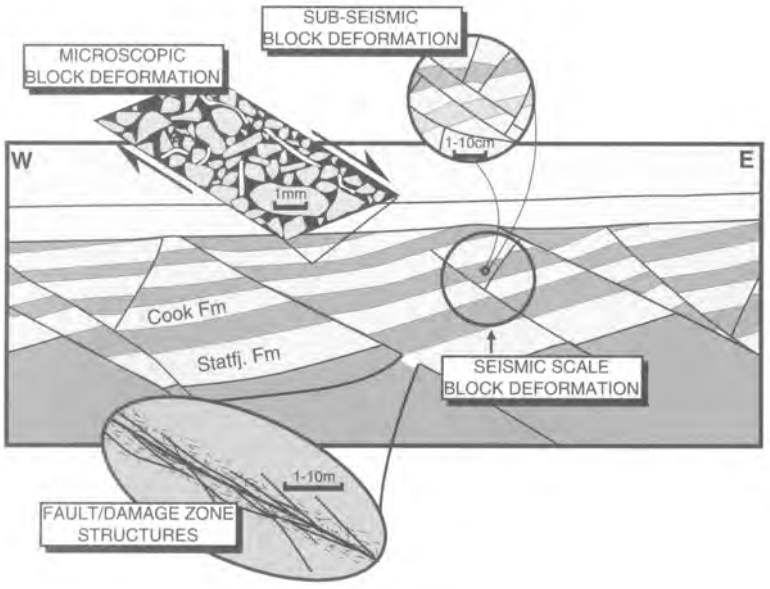

Fig. 28. The various expressions of small-scale deformation in the domino area. See text for discussion.

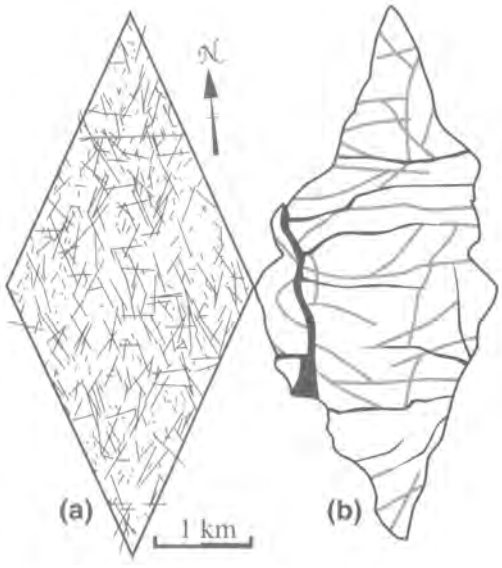

Fig. 29. (**a**) Result of numerical simulation of fault/fracture pattern in fault block B (Fig. 5) (redrawn from Koestler *et al.* 1994). (**b**) Recently remapped fault pattern of the same block after reprocessing of data and application of attribute analysis. Grey lines indicate lineaments on attribute maps that may or may not represent additional minor faults. See text for discussion.

analyses have been applied to identify small faults. This allows us to test the quality of the numerical simulation, at least for a displacement range of 50–15m.

Comparing the numerical model (Fig. 29a) with the improved seismic interpretation (Fig. 29b) reveals significant differences, particularly regarding the length of the internal faults, but also in terms of orientation. Many of the newly mapped faults are much longer than simulated, and an E–W trend is more clearly present in the seismic interpretation than in the model. In conclusion, the distribution of seismically extractable small faults in the domino area cannot explain the strain variation predicted by the model and the non-planar bedding geometries described above.

Sub-seismic faults would be recorded in the more than 6 km of cores collected from the field. Ongoing core studies have revealed suprisingly few sub-seismic faults and fractures more than 10 m away from seismically mappable faults. It is therefore concluded that much of the internal deformation occurs on the microscale.

Microscale deformation within the domino blocks must have involved rotation and translation (sliding) of individual grains. The overall simple shear displacement field predicted by the proposed shear model (Fig. 27b) is accompanied by anisotropic volume loss resulting from deformation-induced grain packing. Grain reorganization, with little grain-size reducing processes,

is a likely process in unconsolidated, shallowly buried and/or overpressured sediments.

The model predicts a direct relationship between dip of bedding and shear strain (Fig. 27b), which can be used to make a strain map of the domino area. Assuming that the rigid rotation preceded the internal shear deformation, the shear strain is found by the relationship:

$$\gamma = \cot(\delta + \alpha) - \cot(\delta + \alpha') \quad (7)$$

where δ is the dip of the shear plane, α' is the dip of the bedding after the rigid block rotation but prior to the shear deformation, and α is the finite (post-deformation) dip of the bedding. For the special case with the shear plane dipping 60°, a fault cut-off angle of the same magnitude and a rigid block rotation of 30°, the shear strain is simply

$$\gamma = \tan(30° - \alpha) \quad (8)$$

The general model with decreasing dip of beds towards the west across the domino blocks is masked by local deformation associated with minor, block-internal faults. However, in large areas it is possible to apply this simple relationship between dip and shear strain to construct tentative shear strain maps (Fig. 15). This simple relationship between dip and internal block strain is clearly disturbed by minor faults within the domino blocks, and the shear strain values also depend on the orientation of the shear plane (60° in Fig. 15). Nevertheless, it gives a good overview of the general strain distribution in the domino area. Assuming that there is a negative correlation between shear strain and porosity or permeability due to the shear-related packing of grains, the map may be utilized in future well planning. In this perspective, areas of high γ-values are more affected by internal shear and therefore represent areas of reduced permeability and vice versa. The map thus reflects the variation in porosity and permeability due to intra-block shearing which is imprinted on variations caused by sedimentological and diagenetic factors.

Stretching estimates

There are a number of different techniques that may be used to estimate extension in extended terranes, each of which implies certain fundamental assumptions about the deformation history. For the domino area, we have already discussed two different types of models: the rigid and soft domino models. Although the rigid domino model has been shown to be an unrealistic one in the case of Gullfaks, it is still useful to consider this model further because it provides a minimum estimate of extension in the domino area.

The *rigid domino model* assumes that the fault blocks, and therefore also the faults, rotate rigidly so that the angular relationship between faults and bedding is maintained throughout the deformation. If we assume that the bedding and the faults rotated rigidly by an amount of 15° (i.e. assuming initial fault dips of 45°),we can use the general formula:

$$\beta = \sin(\alpha + \theta)/\sin\theta \quad (9)$$

to obtain a minimum estimate for the extension in the domino area (θ = present fault dip, α = dip of bedding). The angular relationships from the domino area on the Gullfaks Field ($\alpha = 15°$, $\theta = 30°$) indicate a β value of 1.41 (i.e. 41% extension). Similar numbers were obtained by summing the fault heaves along interpreted seismic lines (Rannoch Formation) across the domino area, and by plan-view restoration of the top Statfjord map (Rouby *et al.* 1996). If we use the higher dips in the easternmost part of the domino blocks (20°) and correct for compaction, Eqn 9 shows that β could be as high as 1.6 according to this model.

The *soft domino model* implied a (theoretical) rigid rotation of the bedding from horizontal to about 30° (Fig. 25d). The contribution from this rigid rotation part of the deformation can be found from Eqn 9 to be $\beta = 1.7$–1.8 (inserting $\alpha = 28$–$30°$, $\theta = 30°$). The additional heterogeneous shear synthetic to the domino faults (Figs 25e, 27b) implies an additional stretch. The contribution of the shear depends on the shear angle and the lateral and vertical variations in shear strain (see Fig. 27b), which makes it more difficult to estimate. It appears, however, that the soft domino model implies a total extension in the domino area in the order of 80%.

The stretching of the horst area is significantly smaller than in the domino area, both because the faults are steeper and thus contribute less to the total extension of the area, and because little internal ('ductile') strain appears to have occurred. Hence, the total extension of the Gullfaks Field (domino area + horst complex) is less than that of the domino area itself.

Conclusions

The present study of the Gullfaks Field shows the result of a three-stage process: (1) an

integrated analysis of seismic data, well data and other available information, resulting in a detailed structural interpretation; (2) geometric analysis of the interpretation, including analysis of faults and bedding, section balancing techniques, and compaction calculations; (3) application of the results to reservoir development. The result is a much more detailed knowledge about the reservoir. The main conclusions from this study are listed below.

- The Gullfaks Field can be structurally subdivided into a major domino system, an eastern horst complex, and an intermediate accommodation zone with a gentle fold structure.
- The main faults dip *c.* 25–30° to the E in the domino area, and *c.* 65° to the W or E in the horst complex.
- Dips of the minor faults are generally larger than 45°, i.e. significantly steeper than the main domino faults.
- The main faults show increasing complexity towards higher reservoir levels, with the development of hangingwall and/or footwall collapse structures.
- The average dip of the bedding in the domino area is 13.0° and 16.6° for the Rannoch Formation and the Statfjord Formation, respectively. This downward increase in dip is related to a vertical variation in block-internal deformation (large-scale drag) and to a lesser extent to differential post-deformational compaction.
- Large-scale drag affects a significant part of the hangingwall side of the fault block. Local drag in the vicinity of the main faults is more strongly developed, and affects strata in both the hangingwall and footwall of the faults.
- Local drag is detected for more than 50% of the minor faults. However, E–W-oriented minor faults do not exhibit detectable drag.
- As a result of large-scale drag, there is a general decrease in dip to the W within the domino fault blocks. The average dip gradient, which varies from block to block, can be as high as $6° \text{ km}^{-1}$.
- Large-scale drag structures are better developed in the Brent Group than in the deeper formations, and a triangular drag zone is identifiable in cross-section.
- Continuous or 'ductile' deformation, as expressed by both local and large-scale drag, affects a wider zone in the hangingwall to faults than in the footwall.
- Faults and bedding have slightly different strike directions. The rotation of the bedding on Gullfaks is thus thought to be related to the large fault(s) to the west rather than to the main faults within the Gullfaks Field.
- Forward modelling indicates that the domino area and the accommodation zone experienced considerably more internal deformation than the horst complex, and a soft domino model with considerable internal block deformation is suggested to explain the geometrical relationships observed within the domino area.
- The soft domino model (assuming initial fault dips of 60–70°) implies an extension of the domino area that is in the order of 80%, i.e. considerably more than the *c.* 40–50% indicated by the rigid domino model.
- Grain reorganization processes are thought to constitute an important part of the internal block deformation.
- A general relationship is suggested between dip and internal block deformation, and therefore between dip and porosity, in the domino area.

The seismic interpretation from which the data was extracted were interpreted in Statoil, Bergen, by H. Fossen, R. Hansen, J. Henden, J. Hesthammer and A. Thon. We thank Norsk Hydro, Saga Petroleum and Statoil for permission to publish the results of this study. G. Yielding is thanked for constructive comments.

References

ANDERSON, E. M. 1951. *The Dynamics of Faulting*. Oliver & Boyd, Edinburgh.

AXEN, G. J. 1988. The geometry of planar domino-style normal faults above a dipping basal detachment. *Journal of Structural Geology*, **10**, 405–411.

BADLEY, M. E., PRICE, J. D., DAHL, C. R. & AGDESTEIN, T. 1988. The structural evolution of the northern Viking Graben and its bearing upon extensional modes of basin formation. *Journal of Geological Society, London*, **145**, 455–472.

BEACH, A. 1986. A deep seismic reflection profile across the northern North Sea. *Nature*, **323**, 53–55.

BENGTSON, C. A. 1981. Statistical curvature analysis techniques for structural interpretation of dip-meter data. *AAPG Bulletin*, **65**, 312–332.

BINGHAM, C. 1964. *Distributions on the sphere and on the projective plane*. PhD thesis, Yale University.

BLUNDELL, D. J., HURICH, C. A. & SMITHSON, S. B. 1985. A model for the MOIST seismic reflection profile, N Scotland. *Journal of the Geological Society, London*, **142**, 245–258.

CHEENEY, R. F. 1983. *Statistical Methods in Geology*. George Allen and Unwin, Boston.

CHILDS, C., WALSH, J. J. & WATTERSON, J. 1990. A method for estimation of the density of fault displacements below the limits of seismic resolution in reservoir formations. *In*: *North Sea Oil and Gas Reservoirs – II*. Norwegian Institute of Technology, Graham & Trotman, London, 309–318.

DAVISON, I. 1989. Extensional domino fault tectonics: kinematics and geometrical constraints. *Annales Tectonicae*, **III**, 12–24.

—— *et al.* 1994. Geological evolution of the south-eastern Red Sea Rift margin, Republic of Yemen. *Geological Society of Amercia Bulletin*, **106**, 1474–1493.

FOSSEN, H. 1992. The role of extensional tectonics in the Caledonides of South Norway. *Journal of Structural Geology*, **14**, 1033–1046.

—— & RØRNES, A. 1996. Properties of fault populations in the Gullfaks Field, northern North Sea. *Journal of Structural Geology*, **18**, 179–180.

—— & GABRIELSEN, R. H. 1996. Experimental modelling of extensional fault systems. *Journal of Structural Geology*, **18**, 673–687.

——, ODINSEN, T., FAERSETH, R. B. & GABRIELSEN, R. H. in press. Detachments and low-angle faults in the northern North Sea rift system. *In*: NØTTVEDT, A. (ed.) *Integrated Basin Studies: Dynamics of the Norwegian margins*. Geological Society, London, Special Publication.

GABRIELSEN, R. H., FAERSETH, R. B., STEEL, R. J., IDIL, S. & KLØVJAN, O. S. 1990. Architectural styles of basin fill in the northern Viking Graben. *In*: BLUNDELL, D. J. &. GIBBS., A. D. (eds) *Tectonic Evolution of the North Sea Rifts*. Clarendon, Oxford. 158–183.

HIGGS, W. G., WILLIAMS, G. D. & POWELL, C. M. 1991. Evidence for flexural shear folding associated with extensional faults. *Geological Society of Amercia Bulletin*, **103**, 710–717.

HORSFIELD, W. T. 1977. An experimental approach to basement controlled faulting. *Geologie en Mijnbouw*, **56**, 363–370.

HOUSEMAN, G. & ENGLAND, P. 1986. A dynamical model of lithosphere extension and sedimentary basin formation. *Journal of Geophysical Research*, **91**, 719–729.

JACKSON, J. A. 1987. Active normal faults and crustal extension. *In*: COWARD, M. P., DEWEY, J. F. & HANCOCK, P. L. (eds) *Continental Extensional Tectonics*. Geological Society, London, Special Publication **28**, 3–17.

——, WHITE, N. J., GARFUNKEL, Z. & ANDERSON, H. 1988. Relations between normal-fault geometry, tilting and vertical motions in extensional terrains: an example from the southern Gulf of Suez. *Journal of Structural Geology*, **10**, 155–170.

JARVIS, G. & MCKENZIE, D. P. 1980. Sedimentary basin formation with finite extension rates. *Earth and Planetary Science Letters*, **48**, 42–52.

KLEMPERER, S. L. 1988. Crustal thinning and nature of extension in the northern North Sea from deep seismic reflection profiling. *Tectonics*, **7**, 803–821.

KOESTLER, A. G., BULLER, A. T., MILNES, A. G. & OLSEN, T. S. 1994. A structural simulation tool for faulted sandstone reservoirs: exploratory study using field data from Utah and Gullfaks. *In*: AASEN, J. O. *et al.* (eds) *North Sea Oil and Gas Reservoirs – III*. Kluwer, Dordrecht, 157–165.

——, MILNES, A. G. & STORLI, A. 1992. Complex hanging-wall deformation above an extensional detachment – example: Gullfaks Field, northern North Sea:. *In*: LARSEN, R. M. *et al.* (eds) *Tectonic Modelling and its Application to Petroleum Geology*. NPF Special Publication **1**, Elsevier, Amsterdam, 243–251.

KUSZNIR, N. J. & ZIEGLER, P. A. 1992. The mechanics of continental extension and sedimentary basin formation: a simple-shear/pure shear flexural cantilever model. *Tectonophysics*, **215**, 117–131.

MCCLAY, K. R. & ELLIS, P. G. 1987. Geometries of extensional fault systems developed in model experiments. *Geology*, **15**, 341–344.

——, NORTON, M. G., CONEY, P. & DAVIS, G. H. 1986. Collapse of the Caledonian orogen and the Old Red Sandstone. *Nature*, **323**, 147–149.

MANDL, G. 1987. Tectonic deformation by rotating parallel faults: the "bookshelf" mechanism. *Tectonophysics*, **141**, 277–316.

PERRIER, R. & QUIBLIER, J. 1974. Thickness changes in sedimentary layers during compaction history: methods for qualitative evaluation. *AAPG Bulletin*, **58**, 507–520.

PETTERSON, O., STORLI, A., LJOSLAND, E. & MASSIE, I. 1990. The Gullfaks Field: geology and reservoir development. *In*: *North Sea Oil and Gas Reservoirs – II*. Norwegian Institute of Technology. Graham & Trotman, London, 67–90.

PRICE, N. J. & COSGROVE, J. W. 1990. *Analysis of Geological Structures*. Cambridge University Press, Cambridge.

RAMSAY, J. G. 1967. *Folding and Fracturing of Rocks*. McGraw-Hill, New York.

ROBERTS, A. M. & YIELDING, G. 1993. Continental extensional tectonics. *In*: HANCOCK, P. L. (ed.) *New Concepts in Tectonics*. Pergamon, Oxford.

——, ——, KUSZNIR, N. J., WALKER, I. M. & DORN-LOPEZ, D. 1995. Quantitative analysis of Triassic extension in the northern Viking Graben. *Journal of the Geological Society, London*, **152**, 15–26.

ROUBY, D., FOSSEN, H. & COBBOLD, P. 1996. Extension, displacements and block rotations in the larger Gullfaks area, northern North Sea, as determined from plan view restoration. *AAPG Bulletin*, **80**, 875–890.

VENDEVILLE, B., COBBOLD, P. R., DAVY, P., BRUN, J. P. & CHOUKROUNE, P. 1987. Physical models of extensional tectonics at various scales. *In*: COWARD, M. P., DEWEY, J. F. & HANCOCK, P. L. (eds) *Continental Extensional Tectonics*. Geological Society, London, Special Publication, **28**, 95–107.

WALSH, J. J. & WATTERSON, J. 1988. Dips of normal faults in British coal measures and other sedimentary sequences. *Journal of the Geological Society, London*, **145**, 859–873.

WESTAWAY, R. & KUSZNIR, N. 1993. Fault and bed "rotation" during continental extension: block rotation or vertical shear? *Journal of Structural Geology*, **15**, 753–770.

WHITE, N. J., JACKSON, J. A. & MCKENZIE, D. P. 1986. The relationship between the geometry of normal faults and that of the sedimentary layers in the hanging walls. *Journal of Structural Geology*, **8**, 897–909.

WITHJACK, M. O., ISLAM, Q. T. & LA POINTE, P. R. 1995. Normal faults and their hanging-wall deformation: an experimental study. *AAPG Bulletin*, **79**, 1–18.